Chinese Chemical Letters 37 (2026) 111831

Contents lists available at ScienceDirect

Chinese Chemical Letters

journal homepage: www.elsevier.com/locate/cclet

Molecular engineering strategies of ammonium vanadates for advanced zinc-ion storage

Kang Zhang[a], Jin Zhao[b,*], Pengcheng Su[a], Mingkun Wang[a], Kexin Wan[a], Hongwei Tang[a], Dai-Huo Liu[a], Jingyu Sun[b,*], Yihui Li[a,*]

[a] Collaborative Innovation Center of Henan Province for Green Manufacturing of Fine Chemicals, Key Laboratory of Green Chemical Media and Reactions, Ministry of Education, School of Chemistry and Chemical Engineering, Henan Normal University, Xinxiang 453007, China
[b] College of Energy, Soochow Institute for Energy and Materials InnovationS (SIEMIS), Key Laboratory of Advanced Carbon Materials and Wearable Energy Technologies of Jiangsu Province, Soochow University, Suzhou 215006, China

ARTICLE INFO

Article history:
Received 30 June 2025
Revised 8 September 2025
Accepted 11 September 2025
Available online 11 September 2025

Keywords:
Molecular engineering strategies
Ammonium vanadates
Zinc-ion storage
Structural modulation
Enhanced transfer kinetics

ABSTRACT

Aqueous zinc-ion batteries (ZIBs) have gained tremendous interests by virtue of their intrinsic safety, low cost and favorable theoretical capacities. As the promising candidates of cathode materials of ZIBs, ammonium vanadates (NVO) have captured widespread attentions owing to their tunable chemical properties and enhanced structural stabilities owing to the existence of NH_4^+ in the $[VO]_n$ layers. However, the pristine NVO fails to meet the expectations due to the strong interlayer electrostatic repulsion and comparatively sluggish transfer kinetics, which necessitates the exploration of appropriate modification strategies to fully dig its potential. Herein, this review systematically summarizes five core molecular engineering strategies, intercalation, defect, interfacial, doping, and structural engineering strategies, and their significances in modulating structural and electrochemical properties of NVO are elaborately discussed. Moreover, the perspectives on the future developments and potential energy-related applications of NVO are presented. This review is anticipated to deepen the researchers' understandings of the potentials of molecular engineering strategies on improving zinc-ion storage capabilities of cathode materials, and further promote the practicality of NVO in ZIBs.

© 2026 Published by Elsevier B.V. on behalf of Chinese Chemical Society and Institute of Materia Medica, Chinese Academy of Medical Sciences.

1. Introduction

The severe fossil fuel consumption and the goal of realizing carbon neutrality readily accelerate the development of sustainable and clean energy [1], and the high-efficient electrochemical energy storage (EES) devices are regarded as the most promising resorts to fulfill the escalating demands of new-energy vehicles and portable electronic devices [2,3]. Up to now, various metal-ion-battery systems have been developed for EES devices (Fig. 1a). As the representative of metal-ion batteries, lithium-ion batteries (LIBs) have been widely commercialized owing to their comparatively high energy density and favorable operation life [4]. Nevertheless, the safety concerns causing by the adoption of flammable organic electrolyte and high cost hamper their further rise in grid-scale EES systems and hybrid vehicles, and the chase of inherently safe EES devices promotes the research progress of aqueous metal-ion batteries [5,6]. In particular, aqueous zinc-ion batteries (ZIBs) have gained tremendous interests by virtue of their comparatively low redox potential (−0.76 V *vs.* standard hydrogen electrode), low cost and desirable theoretical capacity (820 mAh/g) [7,8]. Besides, the favorable air stability and facile assembly procedures further facilitate the industrialization of ZIBs, making them as the competitive candidates for next-generation large-scale grid EES devices [9]. Up to now, numerous cathode materials of ZIBs have been developed, such as vanadium-based cathodes [10–12], manganese-based cathodes [13–15], Prussian blue analogs (PBAs) [16,17], transition metal dichalcogenides (TMDs) [18–20], and emerging organic electrodes [21–23]. Compared to other reported cathodes, vanadium-based cathodes possess favorable capacities and acceptable voltage plateaus (Fig. 1b), enabling them to be one of the most competitive candidates for the cathode materials of ZIBs. However, vanadium-based cathodes generally suffer from the severe structural variations due to the inevitable vanadium dissolution and the sluggish transfer kinetics of Zn^{2+} (zinc-ions) causing by the strong electrostatic repulsion and solvation/desolvation effects, thereby resulting in the inferior cycling stability and failing to meet their expecta-

* Corresponding authors.
E-mail addresses: jzhaoenergy@stu.suda.edu.cn (J. Zhao), sunjy86@suda.edu.cn (J. Sun), liyihui@htu.edu.cn (Y. Li).

https://doi.org/10.1016/j.cclet.2025.111831
1001-8417/© 2026 Published by Elsevier B.V. on behalf of Chinese Chemical Society and Institute of Materia Medica, Chinese Academy of Medical Sciences.

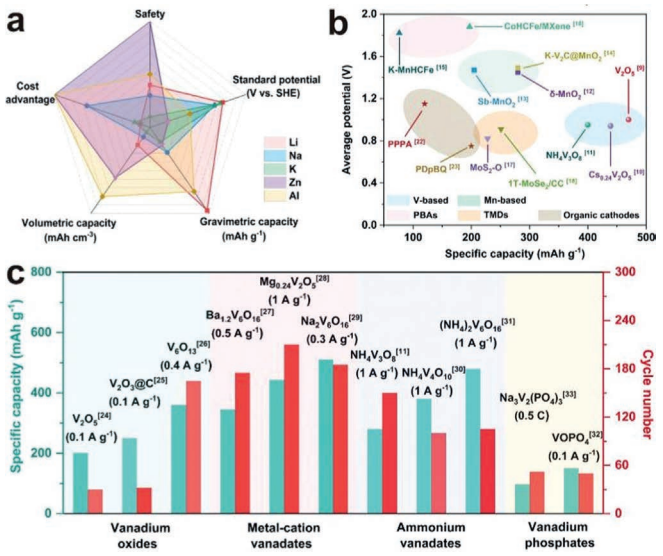


Fig. 1. (a) The radar diagram of various metal-cations as charge carriers for rechargeable batteries. (b) The comparison in the specific capacity and voltage plateau of commonly adopted cathode materials for ZIBs. (c) The comparisons of the initial capacities (0.1 A/g) and cycle numbers to the capacity retention of 80 % of commonly reported vanadium-based cathodes at specific current densities.

Table 1
The structural parameters of several typical NVO materials.

Molecular formula	Interlayer distance (Å)	Crystal system	Bandgap (eV)
$NH_4V_3O_8$	7.9	Monoclinic	1.92
$NH_4V_4O_{10}$	9.6	Monoclinic	1.7–2.1
$(NH_4)_2V_3O_8$	5.6	Tetragonal	1.65–1.9

tions. Consequently, the rational modification strategies are highly desired to realize the favorable cycling stabilities and industrial applications of vanadium-based cathodes.

To date, a series of vanadium-based cathodes have shown their talents in storing Zn^{2+}, such as vanadium oxides [24–26], metal-cation vanadates [27–29], ammonium vanadates (NVO) [11,30,31], and vanadium phosphates [32–34]. By virtue of the enhanced structural stabilities, NVO-based cathodes generally possess the favorable cycling stabilities and Zn^{2+} storage capabilities at high current density compared to vanadium oxides and vanadium phosphates (Fig. 1c). Note that the reported metal-cation vanadates generally possess the better cycle lifespans than pristine NVO by virtue of the higher stabilities of metal-cations in serving as interlayer "pillars". However, the introduction of multivalent metal-cations would further aggravate the electrostatic effect between Zn^{2+} and cathode material, leading to the sluggish transfer kinetics of Zn^{2+}. In contrast, monovalent NH_4^+ can alleviate this adverse effect to some extent, hence, NVO general exhibits the better rate performances than metal-cation vanadates, and the lower cost of its precursor further endows it with favorable commercialization value. Moreover, the lifespan gap between NVO and metal-cation vanadates can be effectively eliminated with the adoption of rational molecular engineering strategies, and the modified NVO-based cathodes are able to present the comparable cycle lifespans to that of metal-cation vanadates, suggesting the great application potentials of NVO in ZIBs.

Specifically, with the common formula of $(NH_4)_xV_yO_z$, NVO is generally comprised of VO_5 square pyramids and VO_6 octahedra or VO_4 tetrahedra with typical layered structures (Table 1 and Fig. 2) [35,36], and it has drawn researchers' attention in recent years by virtue of its tunable structural properties and unique advantages. The NH_4^+ ions are located at the interlayers of $[VO_n]$ layers, and they can form the hydrogen bond network *via* N–H···O bonds, thus greatly strengthening the overall structural stability by serving as extra interlayer "pillars" [37]. Hence, NVO-based electrodes generally possess the better cycling stabilities and long-term cycling performances than pristine vanadium oxide-based electrodes. Moreover, the existence of NH_4^+ ions can further enlarge the interlayer distance of $[VO_n]$ layers, which significantly facilitates the transfer of metal-ions. As a result, NVO-based electrodes have been extensively adopted in numerous EES devices, such as LIBs [38], sodium-ion batteries (SIBs) [39], potassium-ion batteries (PIBs) [40], and supercapacitors (SCs) [41]. However, the potentials of NVO in storing Zn^{2+} have been not revealed until 2019, Tang *et al.* [30] and Lai *et al.* [42] fabricated $NH_4V_4O_{10}$ flake and $NH_4V_3O_8$ nanobelt serving as cathode materials for ZIBs, respectively, and both the NVO cathodes present the reversible intercalation/deintercalation behaviors of Zn^{2+}. Though pristine NVO cathodes with specific morphologies are able to possess enhanced Zn^{2+} storage capabilities [43–45], they still suffer from the following drawbacks: (1) The extra NH_4^+ would further aggravate the electrostatic repulsion between Zn^{2+} and NVO, thus increasing the migration barrier of Zn^{2+} and lowering its transfer kinetics; (2) The NH_4^+ would be inevitably removed during the repeated cycling process, causing the structural collapse and unfavorable cycling stability; (3) The extra NH_4^+ would occupy partial interlayer space and may hinder the transfer of Zn^{2+}, resulting in the sluggish transfer kinetics [11]. Therefore, pristine NVO generally fails to present desirable electrochemical performances, and appropriate modification strategies are highly desired to fully utilize the potentials of NVO cathodes. Aiming to mitigate the above adverse effects of NVO cathodes, significant progress has been made by researchers in recent years, and several related reviews have been published. For instance, Zheng *et al.* elaborately summarized the progress of ammonium salt-based electrodes in the realm of EES [35], and Liu *et al.* discussed the recent progress of vanadium-based cathodes in ZIBs [46]. As one of the most competitive cathode materials of ZIBs, NVO-based cathodes come on stage in recent years, whereas the summaries pertaining to the modification strategies of NVO-based cathodes and relevant discussions in previous reviews are still insufficient and incomplete. Therefore, a review that focuses on summarizing the state-of-the-art modification strategies of NVO and their mechanisms is highly desirable.

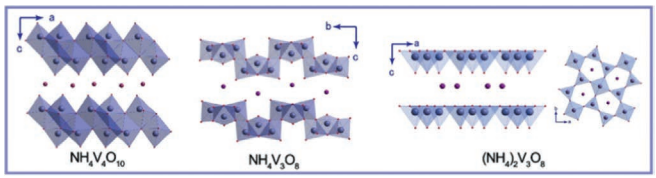


Fig. 2. The crystal structures of the several typical NVO materials. Reproduced with permission [30]. Copyright 2019, The Royal Society of Chemistry.

As the most direct ways to modulate the physical and chemical properties of target material at the molecular level [47], molecular engineering strategies have been adopted for promoting Zn^{2+} storage capabilities of NVO-based cathodes in recent years. In general, the advanced molecular modification strategies of NVO could be roughly classified into four categories according to their principles (Fig. 3), including intercalation engineering, defect engineering and interfacial engineering. Different molecular engineering strategies can promote the electrochemical properties of NVO-based cathodes from different aspects. Besides, these strategies are sometimes compatible, and two or more strategies can be simultaneously adopted by researchers to synergistically alleviate the intrinsic drawbacks of NVO and boost its Zn^{2+} storage capability. Herein,

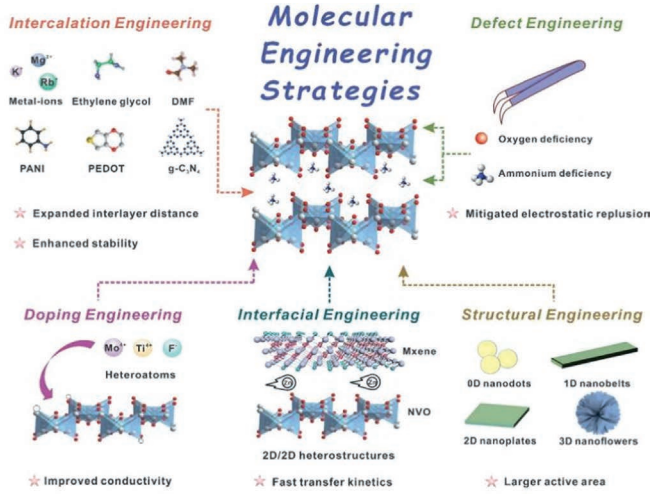


Fig. 3. The general molecular engineering strategies of NVO-based cathodes and their relevant advantages.

for the first time, we systematically summarize the modification strategies of NVO based on previous reports, reveal their intrinsic mechanisms and shed light on the general structural design strategies and applicable prospects of NVO in next-generation EES devices. This review is anticipated to strengthen the comprehension of the structure-activity relationship of NVO-based cathodes, thus making the utmost of the potentials of NVO-based materials and effectively promoting their electrochemical performances in ZIBs and other EES devices.

2. Intercalation engineering

Intercalation engineering is the most common and effective way to promote the electrochemical properties of layered electrodes [48]. Specifically, the adopted intercalators for NVO-based cathodes could be briefly classified into three categories: Metal-ions, organic molecules and conductive polymers, and those intercalators are expected to strengthen the structural stability, increase overall conductivity and contribute more active sites for Zn^{2+} [49]. Herein, the common intercalators are summarized and their individual advantages are discussed in this part.

2.1. Metal-ion intercalator

As one of the most common intercalators for layered materials, metal-ion intercalator is also widely adopted in NVO-based electrodes by virtue of the following advantages: (1) Most of metal-ion intercalators could be easily intercalated into the interlayers of NVO *via* facile hydrothermal/solvothermal methods, suggesting its high feasibility; (2) Metal-ions can further enhance the structural stability of NVO by serving as extra interlayer "pillars"; (3) The intercalated metal-ions are able to modulate the electronic structure of NVO and effectively improve its conductivity. Up to now, numerous metal-ion intercalators have been explored, including alkali-metal-ions (such as Li^+, Na^+, K^+ and Rb^+) [50–56], multivalent metal-ions (such as Mg^{2+} and Ba^{2+}) [57–59], and noble metal-ions [60]. For instance, Cao *et al.* introduced potassium-ions into the interlayers of $NH_4V_4O_{10}$ *via* a facile hydrothermal method (Fig. 4a) [50]. Compared to pristine NVO, the introduction of K^+ significantly reduces the crystallinity of NVO (Fig. 4b), which is beneficial for its long-term cycling stability by mitigating the mechanical stress during electrochemical process. In addition, K^+ can further lower the valance of vanadium and the bond strength of V-O bond (Fig. 4c). Consequently, the proposed K^+-intercalated NVO exhibits the promoted cycling stability, and a high reversible capacity of 172 mAh/g can be retained after 1000 cycles at 5 A/g (Fig. 4d), corresponding to a favorable capacity retention of 81.6%. Similarly, Wang *et al.* adopted Rb^+ intercalator to improve the electrochemical properties of $NH_4V_4O_{10}$ (Fig. 4e) [55]. The introduction of Rb^+ would decrease the interlayer content of labile NH_4^+ and take over the role of interlayer "pillars", resulting in larger content of V^{4+} (Fig. 4f) and expanded interlayer distance (Fig. 4g). Note that the intercalated Rb^+ also contributes to the regulations of electrolyte and zinc anode. Specifically, partial Rb^+-ions would immerse into electrolyte, suppress the generation of byproducts and regulate the growth of zinc dendrite, thus realizing its multi-functionality and superb long-term cycling performance (Fig. 4h). Besides the alkali-metal-ions, multivalent metal-ions are also adopted as intercalators for NVO. Due to their comparatively larger radiuses, the interlayer distances of NVO-based cathodes with multivalent metal-ion intercalators are generally larger than that of alkali-metal-ion intercalated NVO cathodes. Yao *et al.* hired $Mn(CH_3COO)_2$ as the precursor to introduce Mn^{2+} intercalator into $(NH_4)_2V_{10}O_{25}$ [59]. The intercalated Mn^{2+}-ions would partially occupy the accommodation of NH_4^+-ions and serve as new interlayer "pillars" to further strengthen the stability of $[VO]_n$ layers, thus resulting in the enhanced cycling stability. In addition, the appropriate multivalent metal-ion intercalators may also be able to participate in the formation of cathode/electrolyte interface (CEI) layer. Since the stable and uniform CEI layer is vital to the cycling stability of NVO-based cathodes, numerous papers focus on constructing the CEI layer for NVO-based cathodes *via* electrolyte engineering [61] and separator modification strategies [62]. Recently, the Ca^{2+} and Sr^{2+} intercalators have proven their potentials in forming stable CEI layers for vanadium-based cathodes by interacting with electrolytes [63,64]. Therefore, those multivalent metal-ion intercalators may also be able to promote the formation of CEI layer for NVO-based cathodes, while it has been not revealed so far. Nevertheless, the adoption of multivalent metal-ion intercalators may further aggravate the electrostatic repulsion effect between Zn^{2+} and interlayer cations. The electrochemical performances of metal-ion intercalated NVO cathodes are summarized in Table 2, and all the cathodes present much improved cycling stabilities than pristine NVO cathodes. Nevertheless, several issues are needed to be taken into consideration when adopting metal-ion intercalators: (1) Most reported metal-ion intercalations are realized *via* the hydrothermal/solvothermal methods with certain ratios of metal-ion precursors, while not all the metal-ions can intercalate into $[VO]_n$ layers, so how to precisely control and quantify the detailed number of intercalated metal-ions in NVO? (2) The introduction of extra metal-ion would further strengthen the electrostatic repulsion effect between Zn^{2+} and interlayer cations, thereby slacking the transfer kinetics of Zn^{2+}, hence the merits and extra adverse effects contributed by metal-ion intercalators need to be balanced; (3) Most reports focus on revealing the positive influences of metal-ion intercalators on cathodes, while their potential influences on electrolyte and zinc anode need to be further uncovered.

2.2. Organic-molecule intercalator

As the promising alternatives of metal-ions, organic-molecule intercalators have been widely adopted in layered materials (such as TMDs) to mitigate structural variation by serving as the buffer layers [65]. For instance, Zong *et al.* adopted the choline ($C_5H_{14}ON^+$) and Zn^{2+} as intercalators to promote the electrochemical property of layered V_2O_5 [66]. Benefitting from the large "body" of $C_5H_{14}ON^+$, the interlayer distance of V_2O_5 is greatly expanded to 13.5 Å, thus effectively boosting the intercalation/deintercalation processes of Zn^{2+}. However, only a few organic molecules, such as ethylene glycol (EG) and imidazole molecules,

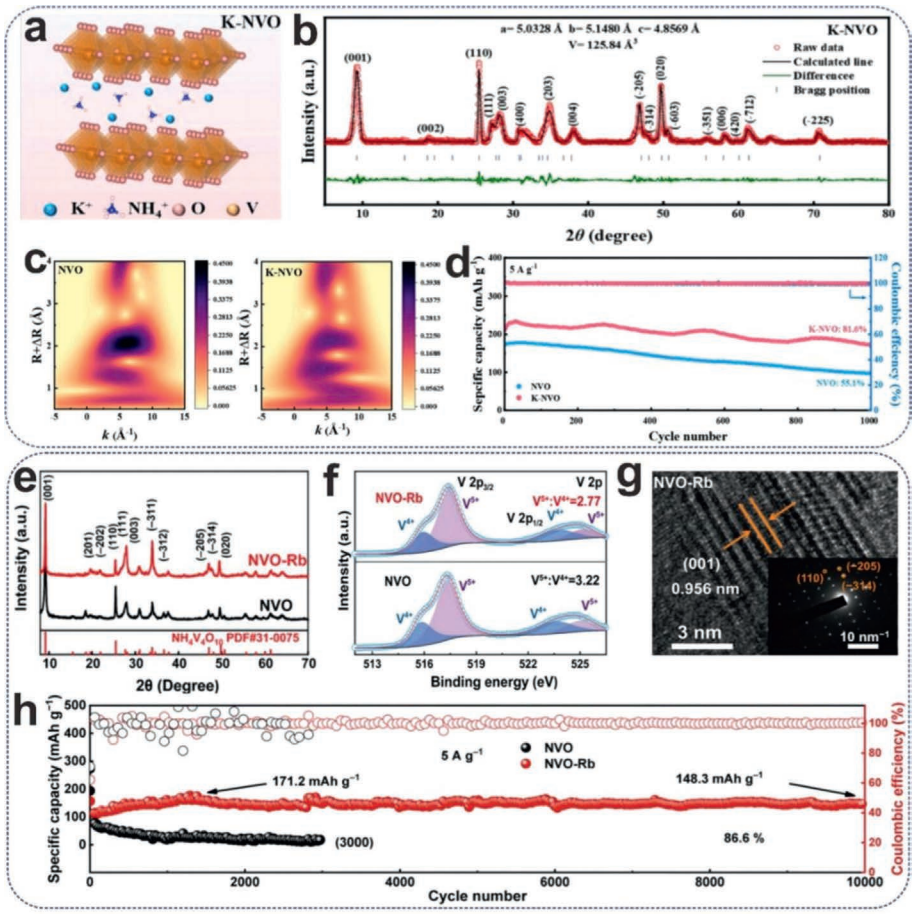


Fig. 4. The typical cases of metal-ion intercalated NVO cathodes. (a) The structure of K-NVO and (b) its XRD spectrum. (c) The EXAFS fitting curves of pristine NVO and K-NVO, and (d) the long-term cycling performance of K-NVO. Reproduced with permission [50]. Copyright 2024, Elsevier Inc. (e) XRD patterns and (f) V 2p spectra of Rb-intercalated NVO and pristine NVO. (g) HRTEM image of Rb-intercalated NVO and (h) its long-term cycling performance. Reproduced with permission [55]. Copyright 2024, American Chemical Society.

Table 2
The electrochemical performances of metal-ion intercalated NVO-based cathodes.

Intercalator	Cathode	Initial capacity (mAh/g) at (*X*) current density	Reversible capacity (mAh/g) after (*Y*) cycles at (*Z*) current density	Ref.
Li^+	Li-$NH_4V_4O_{10}$	486.1 (0.5 A/g)	268.5 (5000) (5 A/g)	[52]
Na^+	Na-$NH_4V_4O_{10}$	400.2 (0.1 A/g)	211 (2000) (10 A/g)	[53]
Na^+	Na-$(NH_4)_{0.5}V_2O_5$	365.4 (0.5 A/g)	245.6 (2000) (5 A/g)	[54]
K^+	K-$NH_4V_4O_{10}$	405 (0.2 A/g)	172 (1000) (5 A/g)	[50]
K^+	K-$NH_4V_4O_{10}$	289.9 (1 C)	236.9 (1000) (5 C)	[51]
Rb^+	Rb-$NH_4V_4O_{10}$	463 (0.1 A/g)	148.3 (10000) (5 A/g)	[55]
Mg^{2+}	Mg-$NH_4V_4O_{10}$	420.5 (0.1 A/g)	152.3 (6000) (5 A/g)	[58]
Ba^{2+}	Ba-$(NH_4)_2V_4O_9$	384.9 (0.1 A/g)	~110 (1500) (5 A/g)	[57]
Mn^{2+}	Mn-$(NH_4)_2V_{10}O_{25}$	355 (0.5 A/g)	162.3 (10000) (20 A/g)	[59]
Ag^+	Ag-$NH_4V_4O_{10}$	473.6 (0.2 A/g)	343.1 (1000) (5 A/g)	[60]

have verified their merits in boosting Zn^{2+} storage capabilities of NVO-based cathodes [67–69]. Organic-molecule intercalators can not only strengthen the structural stability of NVO by serving as interlayer "pillars" and improve the overall conductivity, as well as the metal-ion intercalators, but also possess potential multi-functionalities by virtue of their high polarities and abundant functional groups. Moreover, the introduction of organic molecules could be realized by the facile self-assembly processes, which are more convenient than that of metal-ions. For example, Chen *et al*. introduced the EG molecules into interlayer of $NH_4V_4O_{10}$ *via* facile self-assembly process (Fig. 5a), and its (001) plane shifts from 9.2° (~9.6 Å) to 7.46° (~11.84 Å) after the intercalation of EG (Fig. 5b), corresponding to interlayer distance expansion of ~23 % [67]. Meanwhile, the introduction of EG can greatly reduce the bandgap of NVO from 0.905 eV (pristine NVO) to 0.015 eV, thus improving its electronic conductivity (Figs. 5c and d). As a result, the EG-intercalated NVO delivers a high capacity of 254.8 mAh/g after 1000 cycles at 10 A/g, which is significantly larger than that of pristine NVO cathode. Similarly, Kong *et al.* immersed NVO nanoflake arrays into the *N*,*N*-dimethylformamide (DMF) solution to fabricate DMF-intercalated NVO cathode [70]. The high polarity carbonyl group of DMF can electrostatically interact with NH_4^+ and enable it to be fixed in the $[VO]_n$ layers, while its low polarity alkyl group can attract the Zn^{2+} with the weaker electrostatic effect, thus leading to the fast transfer kinetics of Zn^{2+}. Besides, the interlayer distance of NVO significantly expands to 12.6 Å with in-

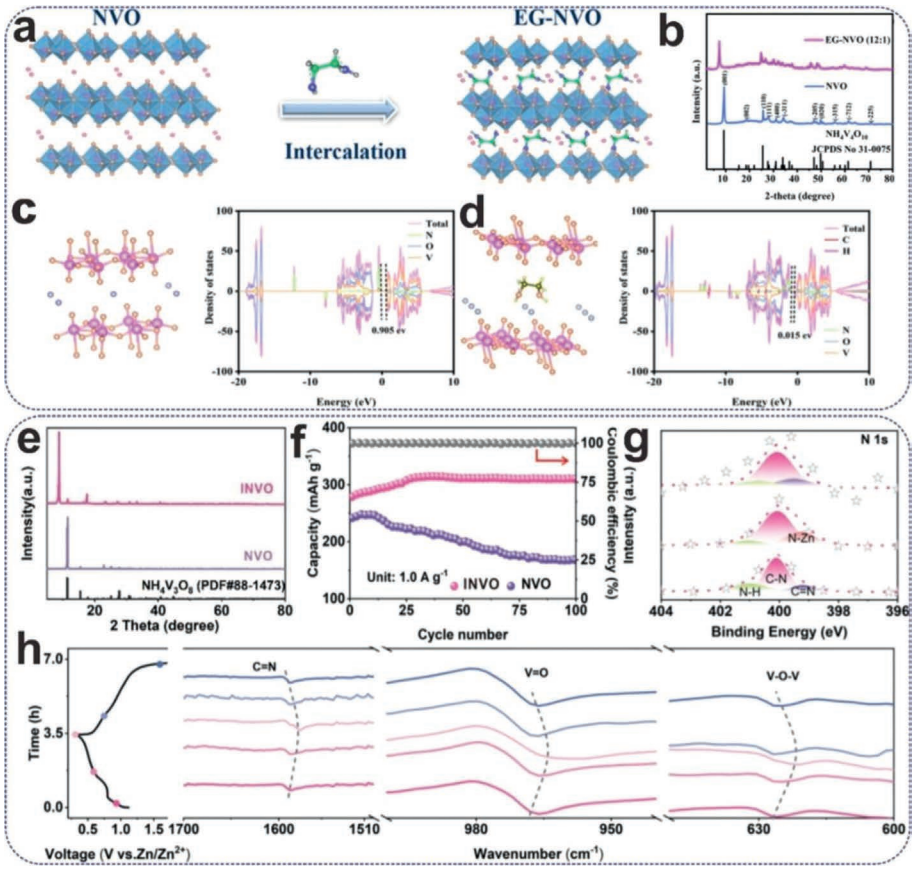


Fig. 5. The typical cases of organic-molecule intercalated NVO cathodes. (a) The structural illustration of EG-intercalated NVO cathode and (b) its XRD patterns. DOS spectra of (c) pristine NVO and (d) EG-intercalated NVO. Reproduced with permission [67]. Copyright 2023, American Chemical Society. (e) XRD spectra and (f) cycling performances of pristine NVO and INVO, the corresponding *ex-situ* (g) XPS spectra and (h) FTIR spectra of INVO. Reproduced with permission [69]. Copyright 2024, American Chemical Society.

Table 3
The electrochemical properties of organic molecule intercalated NVO-based cathodes.

Intercalator	Cathode	Initial capacity (mAh/g) at (*X*) current density	Reversible capacity (mAh/g) after (*Y*) cycles at (*Z*) current density	Ref.
EG	EG-$NH_4V_4O_{10}$	516 (0.5 A/g)	254.8 (1000) (10 A/g)	[67]
EG	EG-$NH_4V_4O_{10}$	427.5 (0.1 A/g)	191.4 (5000) (10 A/g)	[68]
K^+ and EG	K^+, EG-$NH_4V_4O_{10}$	614.1 (0.5 A/g)	472.9 (2000) (10 A/g)	[71]
DMF	DMF-$NH_4V_4O_{10}$	536 (0.5 A/g)	~120 (1000) (5 A/g)	[70]
Imidazole	Imidazole-$NH_4V_3O_8$	400.6 (0.1 A/g)	170.2 (700) (2 A/g)	[69]

tercalation of DMF molecules, further providing the larger space for the accommodation of Zn^{2+}, hence the much-improved Zn^{2+} storage capability of NVO is realized. Besides utilizing the polarities, the functional groups of organic molecules can be also exploited. Tang *et al.* hired imidazole molecule as multifunctional intercalator for NVO cathode [69]. The imidazole molecules can not only serve as interlayer "pillars" to stabilize $[VO]_n$ layers and expand the interlayer distance (Fig. 5e), but also contribute more active sites for Zn^{2+} to storage by virtue of the unique coordination reaction between their C=N group and Zn^{2+}, which are witnessed by the *ex-situ* characterizations (Figs. 5g and h) and thereby realizing the dual-mode Zn^{2+} storage mechanism and enhanced electrochemical performances (Fig. 5f). In addition, organic-molecule intercalator can also collocate with metal-ion intercalator to co-intercalate into the $[VO]_n$ layers of NVO, and synergistically promote its Zn^{2+} storage capability [71]. Up to now, only a few organic molecules have been exploited as intercalators for NVO cathodes (Table 3), and the following issues could be considered aiming to efficiently utilize the organic- molecule intercalators in future: (1) Organic molecules possess various polarities and tunable functional groups that can be exploited, rationally utilizing those characteristics of organic molecules and realizing their multi-functionalities are crucial to the enhancement of Zn^{2+} storage capabilities of NVO cathodes; (2) The content of organic-molecule intercalator is reported to be an influential factor for the structure and morphology of NVO [68], and more detailed researches are highly desired.

2.3. Polymer intercalator

Conductive polymer is another kind of promising intercalators for layered electrodes to enhance their structural stabilities and strengthen the internal conductive networks [72]. In general, the introduction of conductive polymer intercalators can contribute the following advantages for NVO-based cathodes: (1) Significantly expand the interlayer distance of NVO by virtue of their comparatively larger "bodies"; (2) Improve its structural stability by serving as interlayer "pillars" and squeezing out partial NH_4^+ to mitigate the structural collapse causing by the irreversible

Table 4
The electrochemical properties of polymer intercalated NVO-based cathodes.

Intercalator	Cathode	Initial capacity (mAh/g) at (*X*) current density	Reversible capacity (mAh/g) after (*Y*) cycles at (*Z*) current density	Ref.
PANI	PANI-$NH_4V_3O_8$	397.5 (1 A/g)	300 (1000) (10 A/g)	[74]
PANI	PANI-$NH_4V_4O_{10}$	433.78 (0.1 A/g)	308.76 (5000) (5 A/g)	[76]
Na^+, PANI	Na, PANI-$NH_4V_4O_{10}$	610.7 (0.5 A/g)	~250 (5000) (5 A/g)	[73]
Al^{3+}, PANI	Al, PANI-$NH_4V_4O_{10}$	386 (1 A/g)	217 (2000) (5 A/g)	[75]
PPy	PPy-$NH_4V_3O_8$	421 (0.1 A/g)	175.7 (1000) (10 A/g)	[78]
PPy	PPy-$NH_4V_4O_{10}$	431.9 (0.5 A/g)	219.1 (1500) (20 A/g)	[77]
PEDOT	PEDOT-$NH_4V_3O_8$	356.8 (0.05 A/g)	160.6 (5000) (10 A/g)	[79]
PEDOT	PEDOT-$(NH_4)_2V_6O_{16}$	326 (0.5 A/g)	~220 (1000) (10 A/g)	[80]
PoPDA	PoPDA@GO-$NH_4V_3O_8$	433 (0.5 A/g)	167.8 (1000) (5 A/g)	[81]

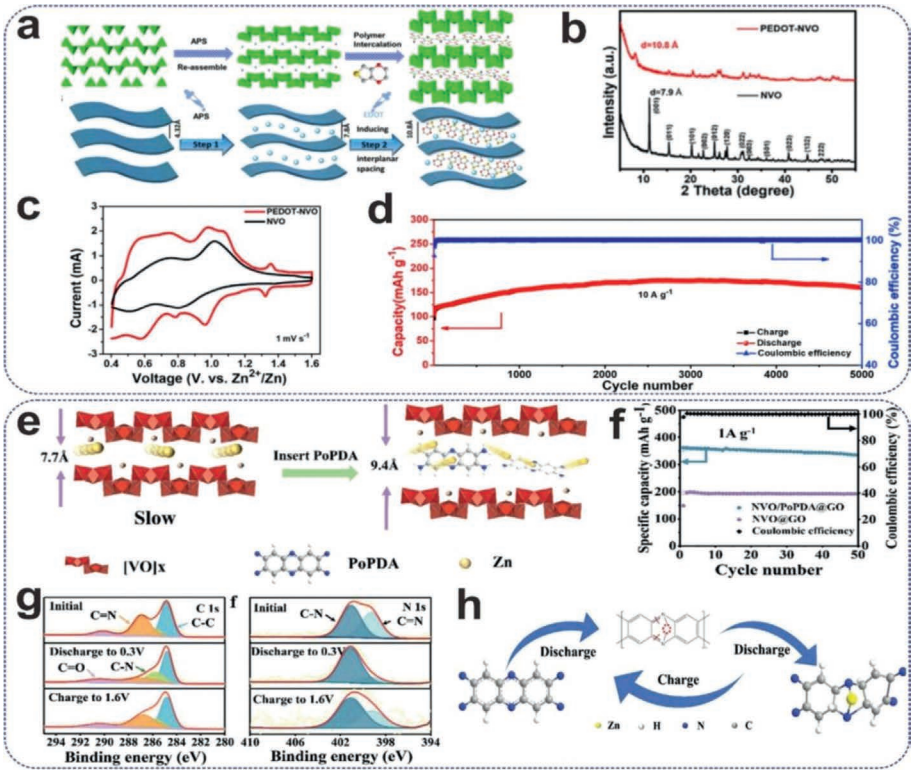


Fig. 6. The typical cases of conductive polymer intercalated NVO cathodes. (a) The fabrication processes of PEDOT-intercalated NVO cathode and (b) its XRD patterns; the comparison of (c) CV curves and (d) long-term cycling performances of pristine NVO and PEDOT-intercalated NVO. Reproduced with permission [79]. Copyright 2020, Elsevier Inc. (e) The enlarged interlayer distance of NVO causing by the intercalation of PoPDA and (f) the electrochemical performances of proposed NVO/PoPDA@GO cathode. (g) The *ex-situ* XPS spectra of NVO/PoPDA@GO cathode and (h) the Zn^{2+} storage mechanism of PoPDA. Reproduced with permission [81]. Copyright 2024, Wiley-VCH GmbH.

deammoniation during cycling process; (3) Enhance its conductivity by contributing the interlayer conductive networks. Up to now, numerous conductive polymers have been adopted as intercalators to promote Zn^{2+} storage capabilities of NVO-based cathodes (Table 4), such as polyaniline (PANI) [73–76], polypyrrole (PPy) [77,78], poly(3,4-ethylenedioxythiophene) (PEDOT) [79,80], and poly-*o*-phenylenediamine (PoPDA) [81]. Early in 2020, Bin *et al*. firstly adopted the PEDOT as intercalator and fabricated PEDOT-intercalated $NH_4V_3O_8$ cathode *via* the ultrasonic-assisted self-assembly process and *in-situ* polymerization process (Fig. 6a) [79]. The introduction of PEDOT effectively expands the interlayer distance of $NH_4V_3O_8$ from 7.9 Å to 10.8 Å (Fig. 6b), thus offering the larger space for the accommodation of Zn^{2+}. Besides, the high conductivity of PEDOT can also contribute to the internal conductive networks, further improving the overall electronic conductivity. As a result, the PEDOT-intercalated NVO cathode presents the larger CV area (Fig. 6c) and boosted Zn^{2+} storage capability compared to pristine NVO cathode. Specifically, it can deliver a superb capacity retention of 94.1 % (160.6 mAh/g) after 5000 cycles at 10 A/g (Fig. 6d), indicating its greatly enhanced structural stability and favorable application potential. Similarly, the introduction of PANI and PPy can also realize the improvement of structural stability and overall conductivity. For example, it is reported that PANI and PPy can expand the interlayer distance of NVO to 10.8 and 8.9 Å from 7.9 Å (pristine $NH_4V_3O_8$), respectively [74,78]. Aiming to further dig the potentials of polymer intercalators, their functional groups could be also exploited. Li *et al*. hired PoPDA as intercalator and fabricated the PoPDA@GO-intercalated $NH_4V_3O_8$ cathode *via* a facile hydrothermal method [81]. In addition to expanding its interlayer distance (Fig. 6e) and enhancing its structural stability by serving as interlayer "pillars", PoPDA can also contribute extra Zn^{2+} storage capacity *via* the coordination reaction between Zn^{2+} and its C=N group, which is similar to that of imidazole intercalator, and the reversible transformation and rearrangement of C=N/C-N-Zn can be verified by relevant *ex-situ* characterizations (Fig. 6g), thereby realizing the organic-inorganic dual-mode active sites for Zn^{2+} to storage (Fig. 6h) and the significantly promoted Zn^{2+} storage capability (Fig. 6f). Moreover, polymer intercalators can also be

adopted together with other intercalators to synergistically boost electrochemical properties of NVO. Zhao *et al*. introduced Na^+ and PANI into the interlayer of $NH_4V_4O_{10}$ simultaneously, and its interlayer distance greatly expanded to 13.8 Å, which is larger than that of mono-intercalator intercalation [73]. As a result, the proposed Na^+ and PANI co-intercalated $NH_4V_4O_{10}$ cathode delivers a favorable capacity retention (92 %, ~250 mAh/g) after 5000 cycles at 5 A/g. However, in consideration of the large "bodies" of polymers, the content of intercalated polymer needs to be carefully considered, since the excessive polymers may block off the interlayer pathways of Zn^{2+} and lead to the sluggish transfer kinetics. In addition, the functional groups of polymers can be also utilized, and developing the conductive polymer intercalators with abundant coordinate sites for Zn^{2+} (such as C=N group) are highly desirable.

2.4. Other intercalator

Besides above intercalators, several inorganic molecules have been also hired as intercalators to boost Zn^{2+} storage capability of NVO. For instance, Xu *et al*. introduced C_3N_4 molecules into the interlayers of V_2O_5 *via* the facile self-assembly process, and C_3N_4 can not only serve as nitrogen source to promote the transformation from V_2O_5 to layered $NH_4V_4O_{10}$ in subsequent hydrothermal procedure, but also play the role of interlayer "pillars" to enhance structural stability of $NH_4V_4O_{10}$ [82]. The C_3N_4-intercalated NVO cathode possesses the larger interlayer distance (10.1 Å) and more oxygen defects, thus presenting boosted Zn^{2+} storage capability, and a high reversible capacity of 219.9 mAh/g can be retained after 10,000 cycles at 10 A/g, suggesting its superb cycling stability. Qiu *et al*. embedded CO_2 molecules into the layers of $NH_4V_4O_{10}$ *via* a self-assembly process and subsequent *in-situ* decomposition of $H_2C_2O_4{\cdot}H_2O$ [83]. The CO_2 molecules can not only expand interlayer distance of NVO, but also immobilize the NH_4^+ *via* hydrogen bonds, thus mitigating structural deformation causing by the deammoniation during cycling processes and guaranteeing the favorable stability of NVO framework. After 1000 cycles at 10 A/g, the proposed CO_2-intercalated NVO cathode maintains a favorable capacity of 214 mAh/g, which is far larger than that of pristine NVO cathode. The above cases indicate the great potentials of inorganic-molecule intercalators in modulating the structural transformation of vanadium-based materials and stabilizing interlayer NH_4^+ "pillars". Nevertheless, compared to organic molecules and polymers, inorganic molecules possess the less functional groups to be modified and exploited, making it hard to realize the multi-functionality of intercalators (such as contribute extra active sites for Zn^{2+} storage), and they generally own the inferior conductivities, which are unfavorable to the overall electron transfer. Hence, inorganic-molecule intercalators may not be as attractive as other types of intercalators.

3. Defect engineering

Defect engineering is another common strategy to modulate electronic structure of NVO and promote its electrochemical performances [84]. Up to now, the proposed defect engineering strategies for NVO could be summarized in two categories: NH_4^+ (cation) defect engineering and oxygen (anion) defect engineering. In general, the existence of NH_4^+ defects can effectively reduce the electrostatic repulsion effect and provide more transfer routes for Zn^{2+} [11], while the introduction of oxygen defects can lower the energy barrier of Zn^{2+} diffusion and facilitate its redox processes [85]. Herein, the introduction methods of those defects and their detailed influences in promoting Zn^{2+} storage capabilities of NVO are elaborately summarized in this part.

3.1. Ammonium-ions defects

The existence of interlayer NH_4^+ "pillars" is vital to maintaining the overall structural stability of NVO during the electrochemical processes. However, the excess number of NH_4^+ would further aggravate the electrostatic repulsion effect between Zn^{2+} and NH_4^+, and occupy the transfer routes of Zn^{2+}, resulting in the inferior transfer kinetics and rate performances [86–88]. Hence, rationally modulating the number of NH_4^+ "pillars" to balance the structural stability of NVO and transfer kinetics of Zn^{2+} can further improve cycling performances and power densities of NVO-based cathodes (Table 5). Moreover, the introduction of NH_4^+ defects can also partially increase the content of V^{5+} in NVO, which is conducive to the redox reactions of vanadium and the increase of electrochemical capacity. In general, the removal of NH_4^+ cations can be realized by the heat treatment or acid treatment. Heat treatment is the most direct way to remove NH_4^+ cations from interlayers of NVO and the heating temperature plays the vital role in modulating the number of removed NH_4^+ cations, since the deficiency of NH_4^+ is proportionate to the calcination temperature and the NVO would completely convert to V_2O_5 at more than 400 °C [89]. Zheng *et al*. prepared NVO nanobelts with abundant oxygen vacancies firstly and removed partial NH_4^+ *via* the mild calcination process at 300 °C (Fig. 7a) [90]. The ratio of NH_4^+ defect is estimated about 12.6 % based on the thermal gravimetric (TG) curve (Fig. 7b) and the variation of N/V ratio of XPS spectrum. The removal of NH_4^+ is proven to be beneficial for the mitigation of interlayer electrostatic interaction and reduction of migration barrier of Zn^{2+}. Consequently, the NH_4^+-deficient $NH_4V_4O_{10}$ cathode possesses an initial capacity of 355 mAh/g at 0.3 A/g (Fig. 7c), and maintains a favorable capacity of 202 mAh/g after 1000 cycles at 3 A/g (Fig. 7d), which is far larger than that of pristine NVO and excessively calcined NVO (which is already transformed to vanadium-based oxide). Similarly, Liu *et al*. further verified the removal necessity of NH_4^+, and they suggested that the N atom of NH_4^+ possesses strong electrostatic interaction with Zn, which would significantly retard the transfer of Zn^{2+} during electrochemical processes [86]. Aiming to further expand the interlayer distance of NVO and compensate the structural variation causing by the partial removal of NH_4^+, the Al^{3+} was pre-intercalated into the $[VO]_n$ layers (AlNVO). As a result, the proposed NH_4^+-deficient AlNVO cathode owns the enhanced Zn^{2+} storage capability and cycling stability than pristine NVO, suggesting the compatibility of NH_4^+-defect engineering with other molecular engineering strategies. Note that the optimal calcination temperature may vary from the detailed structure of NVO. The optimal annealing temperature of $NH_4V_4O_{10}$ is reported to be 300 °C, while Tang *et al*. indicated that the $NH_4V_3O_8$ cathode which is calcined at 350 °C possesses the optimal degree of NH_4^+ defects (~68.5 % based on the calculation of N/V ratio) and upmost electrochemical performance, compared to those $NH_4V_3O_8$ cathodes calcined at 325 and 375 °C [11]. Another advantage of heating treatment method is that the extra oxygen defects can be also generated during the calcination process, which is also in favor of the promotion of Zn^{2+} storage capabilities of NVO. The emergence of oxygen defects can further alleviate the interlayer electrostatic effect between V-O layer and Zn^{2+} and enhance the conductivity of NVO, thus synergistically boosting the Zn^{2+} transfer kinetics with ammonium-ion defects [90]. However, the ammonium-ion defects and oxygen defects will simultaneously emerge in the heating treatment process, and it may be hard to evaluate the specific contribution of ammonium-ion defects and oxygen defects individually. Besides the heat treatment method, acid treatment is also capable to realize the removal of NH_4^+. Chen *et al*. hired the hydrochloric acid to remove partial NH_4^+ from $NH_4V_4O_{10}$ *via* the facile stirring process (Fig. 7e), and the removal degree of NH_4^+ is highly relative to the content of HCl [88]. With the increased con-

Table 5
The electrochemical properties of NH_4^+-deficient NVO-based cathodes.

Material	Defect ratio	Method	Initial capacity (mAh/g) at (*X*) current density	Reversible capacity (mAh/g) after (*Y*) cycles at (*Z*) current density	Ref.
$NH_4V_4O_{10}$	~45 %	Heat treatment (300 °C)	457 (0.1 A/g)	227 (1000) (2 A/g)	[89]
$NH_4V_4O_{10}$	12.6 %	Heat treatment (300 °C)	355 (0.3 A/g)	202 (1000) (3 A/g)	[90]
$NH_4V_4O_{10}$	\	Heat treatment (300 °C)	371 (0.1 A/g)	131 (1000) (5 A/g)	[87]
Al-$NH_4V_4O_{10}$	\	Heat treatment (300 °C)	531.1 (0.2 A/g)	~155 (1400) (10 A/g)	[86]
$NH_4V_3O_8$	68.5 %	Heat treatment (350 °C)	445 (0.1 A/g)	363 (1000) (2 A/g)	[11]
$NH_4V_4O_{10}$	17.9 %	Acid treatment	472.5 (0.1 A/g)	219.5 (2000) (5 A/g)	[88]

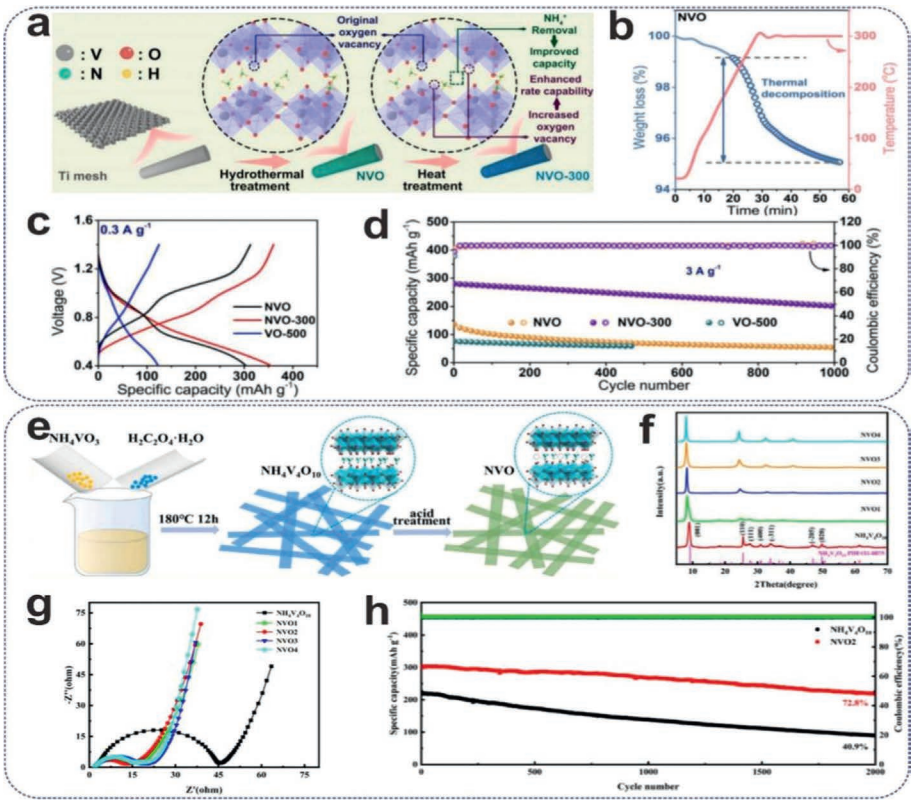


Fig. 7. The typical cases of NH_4^+-deficient NVO cathode. (a) The illustration of NVO-300 cathode with oxygen vacancies and NH_4^+ defects and (b) its TG curve. (c) The initial charge-discharge curve of NVO-300 and (d) its long-term cycling performances. Reproduced with permission [90]. Copyright 2022, Elsevier B.V. (e) The fabrication processes of NH_4^+-deficient NVO cathode *via* acid treatment. (f) XRD spectra and (g) EIS spectra of NVO samples with various acid contents. (h) The long-term cycling performances of NH_4^+-deficient NVO and pristine NVO. Reproduced with permission [88]. Copyright 2022, Elsevier B.V.

tent of HCl, the (001) peak gradually shifts to the lower position, indicating the enlarged interlayer distance (Fig. 7f). Though the excess removal of NH_4^+ can lead to the larger interlayer distance of NVO, its Zn^{2+} transfer kinetics is inferior to the NVO cathode with moderate NH_4^+ defects (Figs. 7g and h), which may be due to the structural deterioration (or transformation) of NVO causing by the excess removal of NH_4^+. In conclusion, NH_4^+ defects can effectively weaken the interlayer electrostatic repulsion effect and expand the interlayer distance, while the excess removal of NH_4^+ may cause the structural deformation and impede Zn^{2+} diffusion. Hence, the optimal degrees of NH_4^+ defects for various NVO materials need to be further revealed, and an approach that can precisely regulate the number of NH_4^+ defects is highly desired.

3.2. Oxygen defects

Oxygen defects can not only effectively modulate electronic structure of NVO and improve its intrinsic conductivity, but also provide more active sites for Zn^{2+} to storage and thereby boosting its electrochemical capacity (Table 6). Moreover, the introduction of oxygen defects is suggested to be beneficial to the inhibition of vanadium dissolution [91]. Generally, oxygen defects can be created *via* one-step hydrothermal method directly or extra reduction process, and various reductants have been adopted for NVO up to now, such as $N_2H_4·H_2O$ [92], thiourea [93], and glucose [94]. He *et al.* hired oxalic acid as the reductant to prepare oxygen-deficient $NH_4V_4O_{10-x}$ microspheres *via* the facile one-step hydrothermal approach (Fig. 8a) [85]. The removal of high-electronegative oxygen can not only alleviate the strong interaction between Zn^{2+} and NVO host and accelerate the intercalation/deintercalation processes of Zn^{2+}, but also provide extra pathways for Zn^{2+} along *c* axis in its layer structure [95,96], thus leading to the much enhanced transfer kinetics of Zn^{2+}. Note that the fast Zn^{2+} transfer kinetics of proposed oxygen-deficient $NH_4V_4O_{10-x}$ could be maintained even at −30 °C (Fig. 8b). Consequently, it possesses favorable Zn^{2+} storage capability at both room temperature (an initial capacity of 434 mAh/g is achieved at 0.1 A/g, Fig. 8c) and low temperature conditions (a high capacity retention of ~94 % is maintained after 2600 cycles at 2 A/g and −30 °C, Fig. 8d), indicating the merits of oxygen defect engineering in promoting practical application potentials of NVO at extreme working conditions. Bai *et al.* proposed an oxygen-defect regulation strategy by adopting glucose as

Table 6
The electrochemical properties of oxygen-deficient NVO-based cathodes.

Material	Defect ratio	Reductant	Initial capacity (mAh/g) at (*X*) current density	Reversible capacity (mAh/g) after (*Y*) cycles at (*Z*) current density	Ref.
$NH_4V_4O_{10}$	1.5 %	Oxalic acid	434 (0.1 A/g)	281.4 (1000) (2 A/g)	[85]
K-$NH_4V_4O_{10}$	\	\	380.8 (0.5 A/g)	236.9 (1000) (2.5 A/g)	[51]
$(NH_4)_2V_{10}O_{25}$/GO	\	\	418 (0.5 A/g)	238 (10000) (20 A/g)	[91]
$(NH_4)_2V_{10}O_{25}$	20.7 %	$N_2H_4{\cdot}H_2O$	512 (0.3 A/g)	~100 (1000) (5 A/g)	[92]
$(NH_4)_2V_{10}O_{25}$	\	Thiourea	408 (0.1 A/g)	160 (4000) (5 A/g)	[93]
$(NH_4)_2V_{10}O_{25}$	18.5 %	Glucose	331.4 (0.3 A/g)	78.3 (7500) (4.8 A/g)	[94]
$NH_4V_4O_{10}$	26.2 %	Oxalic acid	489 (0.5 A/g)	198 (8000) (15 A/g)	[97]

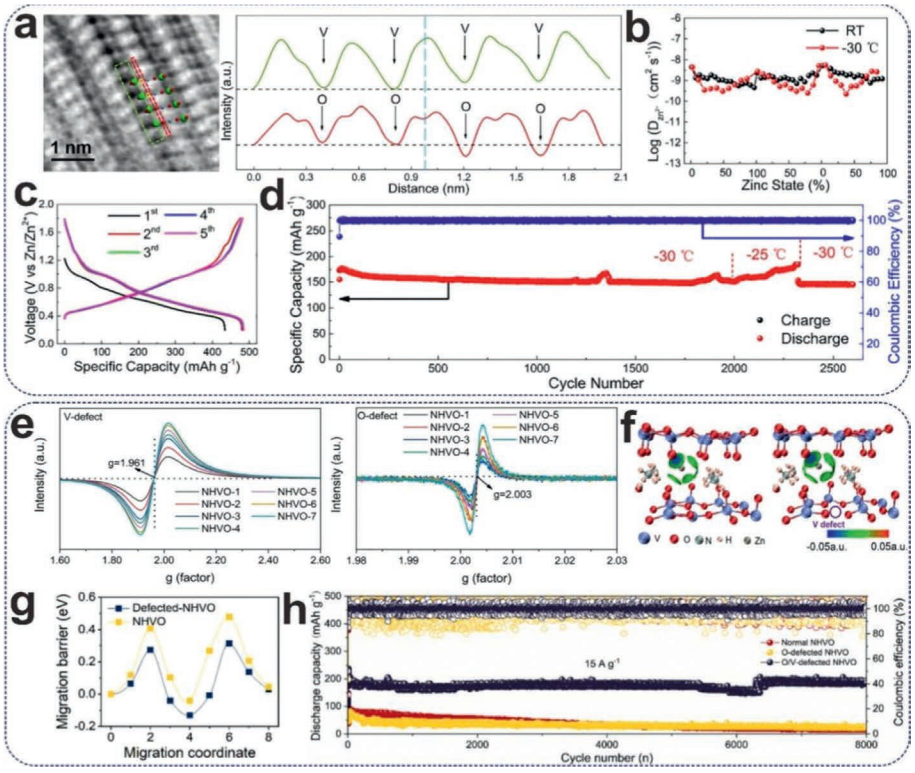


Fig. 8. The typical cases of oxygen-deficient NVO cathode. (a) The STEM image of oxygen-deficient $NH_4V_4O_{10}$ and its corresponding intensity line profile and (b) its calculated Zn^{2+} diffusion coefficients at room temperature and −30 °C. (c) The discharge-charge curves of oxygen-deficient $NH_4V_4O_{10}$ at room temperature and (d) its cycling performance at −30 °C. Reproduced with permission [85]. Copyright 2020, Elsevier B.V. (e) The EPR spectra of V and O of proposed $NH_4V_4O_{10}$. (f) The weak interaction structure between Zn^{2+} and oxygen-deficient $NH_4V_4O_{10}$ and (g) its calculated energy barrier of Zn^{2+} migration. (h) The comparison of long-term cycling performances of proposed NVO electrodes. Reproduced with permission [97]. Copyright 2023, Elsevier B.V.

reductant, and its aldehyde group can grab the lattice oxygen of NVO to form the carboxyl group and generate defects during hydrothermal process [94]. The number of oxygen defect is increased with the increased content of glucose reductant, and those introduced oxygen defects can effectively reduce the bandgap of pristine $(NH_4)_2V_{10}O_{25}$ from 1.9 eV to direct bandgap, confirming the enhanced conductivity of NVO contributed by oxygen defects in theory. However, the excess oxygen defects may also cause structural collapse as well as the NH_4^+ defects, and the optimal Zn^{2+} storage performances are generally owned by those NVO cathodes with moderate oxygen defects. Besides, oxygen defects could be generated with other defects simultaneously under appropriate reductive conditions. Li *et al.* adopted an extra reduction process by using oxalic acid as reductant to simultaneously create oxygen defect and vanadium defect into $NH_4V_4O_{10}$ (Fig. 8e) [97]. The introduction of vanadium defect can weaken the interaction between Zn^{2+} and NVO, thus reducing the binding energy of Zn^{2+} and accelerating its transfer (Fig. 8f), while the existence of oxygen defect is conducive to the increment of 3d electron of V below Fermi energy and the reduction of coordination interaction of Zn-O. The above advantages synergistically endow the proposed vanadium-deficient and oxygen-deficient NVO cathode with the much lower Zn^{2+} migration barrier compared to pristine NVO (Fig. 8g), thereby resulting in the enhanced transfer kinetics. As a result, the NVO cathode with dual defects presents the enhanced apparent diffusion coefficient of 7.5×10^{-10} m^{-2} s^{-1}, which is greatly larger than that of oxygen-deficient NVO (4.5×10^{-10} m^{-2} s^{-1}) and pristine NVO (2.7×10^{-10} m^{-2} s^{-1}). Moreover, though oxygen defects can provide more active sites for Zn^{2+} to storage and improve specific capacity, they are unable to enhance the cycling stability of NVO. However, with the help of vanadium defects, the NVO cathode owns remarkable long-term cycling stability and a high reversible capacity of 210 mAh/g could be retained after 8000 cycles at 15 A/g, indicating the great potential of synergistic effect of multiple defects (Fig. 8h). In summary, the advantages of oxygen-defect strategy on NVO cathode lie in the following aspects: (1) Reduce the bandgap of NVO and improve its conductivity; (2) Weaken the interaction between Zn^{2+} and NVO host, and accelerate intercalation/deintercalation processes of Zn^{2+}; (3) Provide more active sites for Zn^{2+} to storage and improve the specific capacity. How-

ever, the excess number of oxygen defects may lead to the structural collapse and inferior cycling stability, thus the content of oxygen defect in NVO should be elaborately regulated, and a mild method that can precisely control the content of oxygen defect is required. Moreover, since oxygen-defect strategy cannot contribute to the structural stability of NVO, it is better to combine this strategy with other molecular engineering strategies (such as intercalation engineering) in order to strengthen the long-term cycling stability of NVO and obtain the upmost Zn^{2+} storage performance.

4. Interfacial engineering

Interfacial engineering is an extensively adopted modification strategy aiming to modulate or boost the intrinsic properties of target material [98]. Specifically, the adoption of interfacial engineering is expected to contribute the following functions to NVO-based cathodes: (1) Improving the overall conductivity and constructing the conductive network to accelerate the transfer of electron and Zn^{2+}; (2) Strengthening structural stability and mitigating structural variation of NVO during the cycles; (3) Providing abundant active sites or surface area to storage/adsorb the extra Zn^{2+} and promoting the specific capacity. By virtue of its typical 2D layered structure and abundant oxygen groups, it is easy to construct the 2D/2D and 2D/3D heterostructures for vanadium-based oxides *via* the facile hydrothermal/solvothermal methods or self-assembly process [99,100]. Up to now, carbonaceous materials and 2D active materials are the two main categories that adopted for NVO to construct the interfaces, which will be discussed in this section.

4.1. Carbonaceous interface

Carbonaceous materials possess favorable conductivities and surface areas, which enable them to collaborate with active materials to construct conductive network and storage more metalions [101]. Moreover, carbonaceous materials can also enhance the structural stability of host material by serving as buffer layer to alleviate the structural variation during electrochemical processes, or serve as substrate to well disperse host materials and effectively mitigate their aggregation or restacking [102]. In particular, numerous typical carbonaceous materials have been adopted to boost the Zn^{2+} storage capabilities of NVO-based cathodes, such as graphene oxide (GO) [91], reduced graphene oxide (rGO) [103], and carbon nanotube (CNT) [104]. For instance, Jiang *et al*. hired alkali-treated carbon cloth (ACC) as flexible substrate to disperse the $(NH_4)_2V_{10}O_{25}$ nanosheet [105]. The adoption of ACC substrate effectively mitigates the aggregation of NVO and construction of conductive interfacial between ACC and NVO guarantee the fast transfer of electron, thus presenting favorable cycling stability and a high capacity retention of 93.4% can be achieved after 1000 cycles at 2 A/g. In addition, Jiang *et al*. used multi-walled CNTs as substrate to grow $(NH_4)_{0.38}V_2O_5$ nanoribbons serving as binder-free freestanding cathode [104]. Similarly, the high conductivity and abundant pores of CNT guarantee the favorable transfer of electron and electrolyte filtration between the interfacial of NVO and CNT substrate, thereby resulting in the enhanced cycling stability and energy density of 343 Wh/kg at a power density of 110 W/kg. In addition to constructing the 2D/3D interfaces, NVO can also form the 2D/2D heterostructure interface with 2D carbonaceous materials. Liu *et al*. prepared the $NH_4V_4O_{10}$/rGO heterostructure *via* the microwave-assisted chemical deposition method [106]. The introduction of rGO interface can not only expand the interlayer distance of $NH_4V_4O_{10}$ from 9.76 Å to 10.82 Å, but also effectively reduce the bandgap of NVO by virtue of the orbital hybridization effect between the 2p orbitals of O atom from NVO and C atom from rGO, leading to the metallic properties of NVO/rGO heterostructure. Those advantages enable NVO/rGO composite cathode to possess much larger Zn^{2+} diffusion coefficients and enhanced long-term cycling performances than pristine NVO cathode, indicating the significance of introducing conductive interface on improving Zn^{2+} storage capability of NVO. Likewise, the construction of NVO/carbonaceous interface can also collaborate with other strategies to realize the exertion of multiple molecular engineering strategies (such as defect engineering) and achieve the better electrochemical performances than that of single strategy [107]. Moreover, the carbonaceous interface is also expected to be served as extra CEI layer to further enhance the stability of NVO. Li *et al*. pre-implanted the amorphous carbon interface into MnV_2O_4 to be served as CEI layer, and the constructed MnV_2O_4@C heterostructure exhibits the favorable zinc-ion storage capability and cycling stability by virtue of the introduced hydrophobic and conductive CEI layer [108]. This strategy may be also suitable for the NVO-based cathodes. Moreover, an extra built-in electric field is also verified in the NVO/CC interface [109], and the existed interfacial electrical field may also contribute to the formation and stabilization of CEI layer. Unfortunately, the relevant researches are still insufficient, and more papers are required to further reveal the potential of interfacial engineering strategy on constructing the CEI layers for NVO-based cathodes.

4.2. 2D material interface

By virtue of its typical 2D layered characteristic and abundant oxygen content, NVO can form the 2D/2D heterostructure with other 2D conductive materials beyond 2D carbonaceous materials easily. By coupling with 2D functional materials, the electronic structure of NVO can be elaborately modulated. In addition, 2D active materials can provide more sites for Zn^{2+} to storage and improve the overall capacity. However, only a few 2D functional materials have been adopted to construct heterostructure interfaces with NVO (Table 7), such as MXene and MoS_2 [110–112]. As an emerging 2D layered material, MXene owns favorable conductivity and abundant surface functional groups, enabling it to be extensively used in energy-related applications [113]. In particular, the NVO/MXene heterostructure could be prepared *via* the facile self-assembly method or vacuum filtration process, and the intrinsic flexibility of MXene film can generally endow the NVO/MXene composite with favorable potentials in flexible energy storage devices. Qi *et al*. fabricated the freestanding $(NH_4)_2V_{10}O_{25}$@MXene heterostructure film *via* a facile vacuum filtration method [114]. The unique hierarchical structure of this NVO@MXene hybrid film can provide more active sites for Zn^{2+} and the conductive network of MXene shell guarantees the fast transfer kinetics of electron and Zn^{2+}, thus resulting in the enhanced Zn^{2+} diffusion coefficient (10^{-10}-10^{-11} cm^2/s) than pristine NVO cathode. Nie *et al*. constructed the $NH_4V_4O_{10}$@MXene heterojunction through the electrostatic self-assembly process (Fig. 9a) [111]. The interlaminar MXene nanosheets are able to maintain the stability of expanded layered structure of NVO during cycling processes. Moreover, their favorable conductivities further enrich the interlayer conductive networks and facilitate the Zn^{2+} transfer process, leading to the significantly decreased diffusion barrier of Zn^{2+} (Fig. 9b). Consequently, the proposed NVO@MXene heterostructure delivers favorable long-term cycling stability and rate performance. Specifically, a high reversible capacity of 110 mAh/g can be sustained after 2000 cycles at 5 A/g (Fig. 9c), with the smooth and flawless electrode surface morphology, verifying the merits of those introduced MXene interfaces in alleviating structural collapse during electrochemical processes. Moreover, introducing extra MXene-based heterostructure interfaces is suggested to be beneficial to enhance the stability of oxygen defects of vanadium oxide [115], which may be also suitable for that of NVO-based cathodes and further pro-

Table 7
The electrochemical properties of NVO-based cathodes with 2D-material interfaces.

Material	NVO content (wt%)	Initial capacity (mAh/g) at (*X*) current density	Reversible capacity (mAh/g) after (*Y*) cycles at (*Z*) current density	Ref.
$(NH_4)_2V_{10}O_{25}$@$Ti_3C_2T_x$	70	514.7 (0.1 A/g)	105.6 (6000) (5 A/g)	[110]
$(NH_4)_2V_{10}O_{25}$@$Ti_3C_2T_x$	70	498 (0.5 A/g)	151 (1000) (5 A/g)	[114]
$NH_4V_4O_{10}$@$Ti_3C_2T_x$	~98	~210 (1 A/g)	110 (2000) (5 A/g)	[111]
$(NH_4)_2V_6O_{16}$/1T MoS_2	~97.1	370.5 (0.2 A/g)	141 (2000) (10 A/g)	[112]

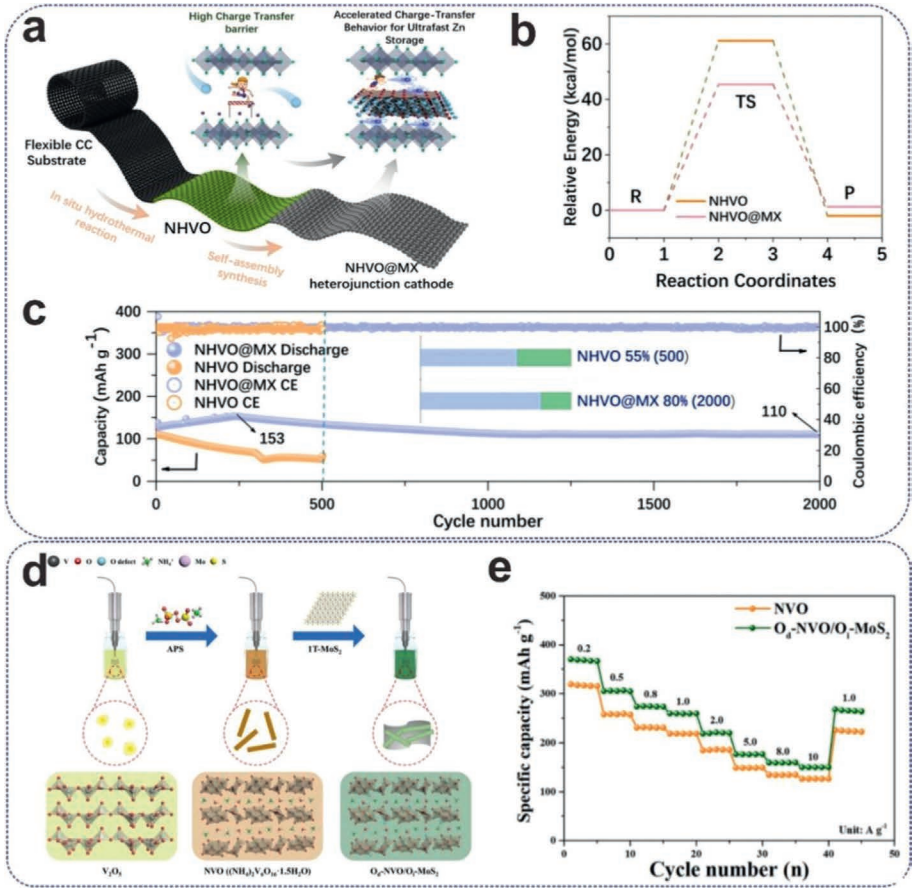


Fig. 9. The typical cases of NVO cathodes with other 2D active material interfacial. (a) The fabrication process of $NH_4V_4O_{10}$@MXene cathode; the comparison of (b) Zn^{2+} diffusion barriers and (c) long-term cycling stability at 5 A/g of $NH_4V_4O_{10}$@MXene and pristine $NH_4V_4O_{10}$. Reproduced with permission [111]. Copyright 2023, Elsevier B.V. (d) The preparation process of 1D/2D NVO nanorod/MoS_2 composite and (e) its rate performance. Reproduced with permission [112]. Copyright 2023, Elsevier B.V.

mote the utilization of defect engineering strategy in NVO, and more interfacial functions of MXene are needed to be further explored. In addition to MXene, TMDs have been also adopted to construct the heterostructure interfaces with NVO recently. Lee *et al*. constructed the 1D/2D NVO nanorod/1T MoS_2 nanosheet composite *via* the facile sonication process (Fig. 9d) [112]. The MoS_2 nanosheets with abundant 1T ratio possesses favorable conductivity and hydrophilicity, allowing the fast transfer of Zn^{2+} and electrons in the interfaces of NVO and MoS_2. Besides, MoS_2 can also provide extra active sites for Zn^{2+} and contribute to the overall capacity. As a result, the NVO@MoS_2 composite exhibits enhanced rate performance (Fig. 9e) and cycling stability. Notably, it is able to present the high capacities of 319.5 and 149.8 mAh/g at 0.2 and 10 A/g, respectively, and maintain the boosted capacity retention of 92.5% after 2000 cycles at 10 A/g. Compared to the carbonaceous interfaces, the utilization of NVO/2D material interface may be able to contribute more advantages beyond improving overall conductivity, such as generate/stabilize extra oxygen defects or modulate the electronic structure of NVO, whereas only a few 2D functional materials have been studied up to now. Hence, the merits of other 2D multifunction active materials in NVO-based cathodes are needed to be further explored.

5. Doping engineering

Doping engineering is an extensively used strategy to tailor the physicochemical properties of electrode materials to perform the enhanced electrochemical performances [116]. Differing from the intercalation engineering strategy (which allows intercalators to insert into the interlayers), doping engineering strategy aims to substitute the target elements with specific dopants or stuff dopants into its lattices. Therefore, doping engineering can directly tailor the electronic structure, and it has been proven to be an effective way to boost the Zn^{2+} storage capabilities of common cathode materials (such as vanadium-based and manganese-based cathodes) [117–119]. In general, the commonly adopted dopants can be classified into two categories: metal-ion dopants and nonmetal dopants (Table 8) [120]. Based on the previous reports, the introduction of heteroatom dopants normally will not alter the pristine crystal structures of NVO, which may be due to their comparatively

Table 8
The electrochemical properties of metal-ion and nonmetal-ion doped NVO-based cathodes.

Material	Dopant content	Dopant merit	Reversible capacity (mAh/g) after (*Y*) cycles at (*Z*) current density	Ref.
Mg-doped $NH_4V_4O_{10}$	~6.3 %	Enhance stability, inhibit deammoniation	~180 (5000) (10 A/g)	[121]
Ti-doped $NH_4V_4O_{10}$	~10 %	Enhance stability, inhibit the accumulation of Zn^{2+}	146 (2000) (2 A/g)	[122]
Mo-doped $NH_4V_4O_{10}$	\	Improve conductivity, expand interlayer distance	~250 (500) (0.5 A/g)	[123]
F-doped $NH_4V_4O_{10}$	~6 %	Improve conductivity, tune coordinated environment of V	274 (2000) (4 A/g)	[124]

lower contents (usually less than 10 %). The main influences of dopants on NVO lie in the following two aspects: (1) Conductivity. The specific heteroatom dopants can donate their electrons to NVO and increase the electron density, thus greatly boosting overall conductivity [121]. (2) Morphology. The introduction of dopants can also promote the morphology transformation of NVO and alter its interlayer distance, which enables researchers to optimize the morphology by regulating the content of dopant. Up to now, several metal-ion dopants have proven their merits. He *et al*. fabricated the Ti-doped $NH_4V_4O_{10}$ by using titanium isopropoxide as Ti source [122]. Notably, with the introduction of Ti dopant, the size of NVO nanobelt is greatly reduced, which is expected to promote the electrolyte infiltration and facilitate the diffusion of Zn^{2+}. Consequently, the Ti-doped NVO owns the boosted Zn^{2+} diffusion coefficient (4.2×10^{-10}–9.9×10^{-11} cm^2/s) and cycling stability than pristine NVO (8.8×10^{-11}–1.2×10^{-12} cm^2/s). Wang *et al*. prepared Mo-doped $NH_4V_4O_{10}$ *via* the facile hydrothermal method (Fig. 10a) [123]. Similarly, the introduction of Mo dopant can also alter the morphology of NVO (from nanoplate to nanorod and nanowire with the increased content of Mo dopant) and facilitate electrolyte infiltration. Moreover, by substituting partial V atoms with Mo atoms, the bandgap of pristine NVO is greatly reduced from 2.10 eV (Fig. 10b) to 1.36 eV (Fig. 10c), thus enhancing the overall conductivity. In addition, Mo dopants can also trigger the variation of interlayer distance, which is revealed by the shift of its (001) peak (Fig. 10d). With the increased conductivities and expanded interlayer distances, all the Mo-doped NVO cathodes present larger Zn^{2+} diffusion coefficients than pristine NVO (Fig. 10e), and the optimal cathode retains a reversible capacity of ~250 mAh/g after 500 cycles at 0.5 A/g (Fig. 10f). In addition to metal-ion dopants, the merits of nonmetal-ion dopants in NVO-based cathodes have been also revealed. Unlike the metal-ion dopants, which are served as the substitutes of V atoms, nonmetal-ion dopants generally target at the O atoms, and thus modulating the coordinated environment of V atoms. Zhuang *et al*. hired NH_4F as fluorine precursor to fabricate F-doped $NH_4V_4O_{10}$, and partial oxygen sites are substituted by the F atoms with the higher electronegativity and larger radius (Fig. 10g) [124]. With a substitution content of ~6 %, the proposed NVO exhibits the expansion interlayer distance of 10.5 Å from 9.8 Å (Fig. 10h). Moreover, the introduction of F-dopant can further narrow the bandgap of NVO and increase the density state near the Fermi energy level, resulting in the much-enhanced conductivity (Figs. 10i and j). Benefitting from the above advantages, the F-doped NVO cathode exhibits boosted Zn^{2+} storage capability and cycling stability, it can maintain the reversible capacities of 363 and 274 mAh/g after 100 cycles at 0.1 A/g (Fig. 10k) and 2000 cycles at 4 A/g, respectively, which is far larger than that of pristine NVO. Though nonmetal dopants possess great potentials in ameliorating Zn^{2+} storage capability of NVO, the relevant researches are still insufficient, and the following issues need to be further revealed: (1) The influence of nonmetal dopants on altering the morphology and structure of NVO; (2) The specific relationship between the content of dopant and Zn^{2+} storage capability. Besides, those dopants may able to endow NVO with other unexplored functions. For instance, Deng *et al*. suggested that F dopant can promote the formation of hydrophobic surface on V_2O_5 and inhibit the vanadium dissolution, thus improving the Zn^{2+} storage capability of V_2O_5 [125]. Those advantageous phenomena may be also detected in F-doped NVO materials, while it has not been experimentally substantiated yet.

6. Structural engineering

Structural engineering strategy aims to alleviate the intrinsic drawbacks of active materials by tailoring their morphologies and constructing the optimized stack modes. In general, structural engineering strategies can effectively alter the physical characteristics of active materials, such as active surface area and the conductivity, which are crucial to their electrochemical properties. Specifically, previous researches have suggested that the morphology and structure play the important role in improving lithium-ion storage capability of NVO [126], and various morphologies of NVO have been developed by modulating the fabrication conditions (such as hydrothermal temperature or pH value) [38,127], including nanobelt [128], nanoflake [129], and nanorod [130]. Since the morphologies and structures are vital to the Zn^{2+} storage capabilities of cathode materials [131], those characteristics of NVO-based cathodes need to be elaborately designed to fully utilize their potentials in storing Zn^{2+}. Up to now, various morphologies of NVO-based cathodes have been proposed and their Zn^{2+} storage capabilities are studied (Table 9), including nanoribbons [104], nanoflakes [132], nanobelts [133], and numerous 3D architectures (such as nanoflowers and nanospheres) [134,135]. Up to now, numerous strategies have been proposed to modulate the morphology and structure of NVO. Wang *et al*. fabricated a series of $(NH_4)_2V_4O_9$ samples with various morphologies by adjusting the content of citric acid additive in precursor solution (Fig. 11a) [136]. The introduction of citric acid additive is suggested to be able to increase the coordination number of vanadium-ions, and the addition of a small content of citric acid will inhibit the anisotropic growth of NVO crystal, leading to the structural transformation from nanobelts to square plates. With the increased content of citric acid, citrate will spontaneously cross-link to form the carbon spheres and induce the self-assembly of NVO plates (Fig. 11b). When the vanadium ions are surrounded by excessive citrates, the growth of NVO is further depressed and finally resulting in the formation of nanodots. Moreover, this structural evolution is accompanied by the variation of interlayer distance and the introduction of oxygen defects, which are beneficial to the fast transfer of Zn^{2+}. Consequently, the optimal NVO nanodots exhibit enhanced cycling stability and a favorable capacity retention of 81 % can be achieved after 5000 cycles at 5 A/g (Fig. 11c). Sun *et al*. adopted the self-template strategy to prepare the novel 3D decussate $NH_4V_4O_{10}$ superstructure (Fig. 11d) [137]. Note that the pH value plays a vital role in controlling morphology of NVO, and this self-assembly process can be only triggered when the pH value is larger than 1.7, owing to the improvement of electrical attraction interaction causing by the comparatively larger pH value. Compared to the typical layered structure of NVO, this unique and open 3D decussate structure possesses the larger active surface area and more Zn^{2+} trans-

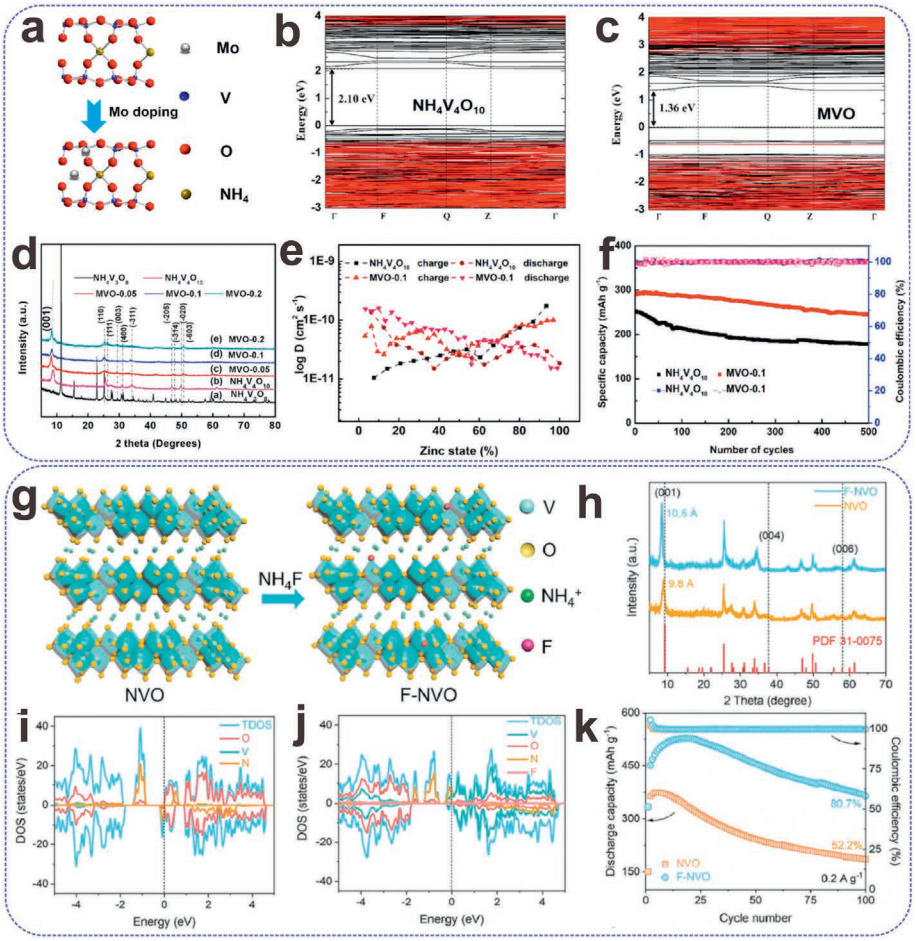


Fig. 10. The typical cases of doping engineering strategies of NVO cathodes. (a) The structure of Mo-doped $NH_4V_4O_{10}$ cathode; the calculated band structures of (b) Mo-doped NVO and (c) pristine NVO. (d) XRD spectra, (e) Zn^{2+} diffusion coefficients and (f) cycling performances of Mo-doped NVO cathodes with various content of Mo dopant at 0.5 A/g. Reproduced with permission [123]. Copyright 2020, Elsevier B.V. (g) The structure of F-doped $NH_4V_4O_{10}$ and (h) its XRD spectrum. The calculated PDOS spectra of (i) pristine NVO and (j) F-doped NVO. (k) The cycling performances of F-doped NVO and pristine NVO cathodes. Reproduced with permission [124]. Copyright 2023, Wiley-VCH GmbH.

Table 9
The electrochemical properties of NVO-based cathodes with specific morphologies and structures.

Material	Initial capacity (mAh/g) at (*X*) current density	Reversible capacity (mAh/g) after (*Y*) cycles at (*Z*) current density	Ref.
$NH_4V_4O_{10}$ nanobelt	457.9 (0.1 A/g)	172.3 (3000) (3 A/g)	[133]
3D flower-like $NH_4V_4O_{10}$	487 (0.1 A/g)	~140 (3000) (10 A/g)	[134]
3D $NH_4V_4O_{10}$ microspheres	522.9 (0.1 A/g)	~90 (20,000) (20 A/g)	[135]
Amorphous $(NH_4)_2V_4O_9$ nanodots	273 (1 A/g)	~150 (5000) (5 A/g)	[136]
3D decussate $NH_4V_4O_{10}$ superstructure	475.8 (0.4 A/g)	221.4 (2100) (5 A/g)	[137]
Nano-array NVO	524 (0.1 A/g)	~100 (1000) (5 A/g)	[138]
$NH_4V_4O_{10}$ nanoflakes/CF	233 (5 A/g)	~116.2 (2500) (20 A/g)	[132]
$(NH_4)_2V_6O_{16}$ nanobelts@rGO	~500 (0.1 A/g)	322 (1000) (5 A/g)	[140]
$(NH_4)_2V_3O_8$ nanoparticle/C	~300 (0.1 A/g)	135 (2000) (1 A/g)	[141]
$(NH_4)_{0.38}V_2O_5$ nanoribbon/CNT	460 (0.1 A/g)	415.2 (500) (0.1 A/g)	[104]

fer channels, thus exhibiting the improved diffusion coefficient of Zn^{2+} ($10^{-8.6}$–$10^{-10.2}$ cm^2/s, Fig. 11e) and Zn^{2+} storage capability. Consequently, this novel 3D structure endows NVO with favorable cycling performances and a superb capacity retention of 90% can be remained after 2100 cycles at 5 A/g (Fig. 11f). In addition to modulating the fabrication parameters (such as precursor content and pH value), the morphology of NVO can be also regulated by the subsequent treatment processing. By adopting the appropriate drying method, the morphologies and structures of NVO products can be tailored [138].

Constructing composite architecture with other conductive materials is another effective structural strategy for NVO to improve its electrochemical properties. As the blue-eyed boy of researchers, carbonaceous material has been extensively adopted to serve as the conductive substrate, coating layer or pillars to disperse active materials and stabilize the overall stability [139]. Up to now, numerous carbonaceous materials have substantiated their merits on improving Zn^{2+} storage capabilities of NVO, such as carbon cloth [105], carbon fiber (CF) [132], and rGO [140]. For instance, Jiang *et al.* adopted the amorphous carbon matrix to encapsulated

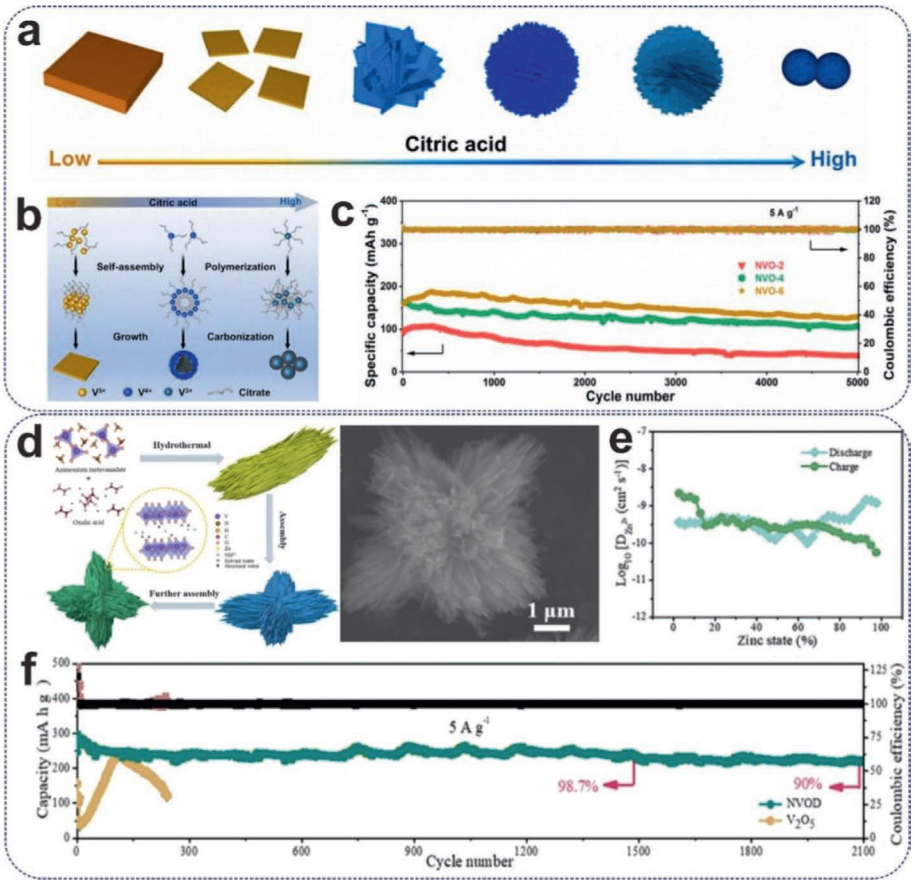


Fig. 11. The typical cases of structural engineering strategies of NVO cathodes. The (a) morphology evolution, (b) the relevant mechanism of NVO with various content of citric acid and (c) their cycling performances at 5 A/g. Reproduced with permission [136]. Copyright 2023, Elsevier B.V. (d) The fabrication process and SEM image of 3D decussate $NH_4V_4O_{10}$, and (e) its calculated Zn^{2+} diffusion coefficient. (f) The long-term cycling performances of 3D decussate $NH_4V_4O_{10}$ at 5 A/g. Reproduced with permission [137]. Copyright 2021, American Chemical Society.

the $(NH_4)_2V_3O_8$ nanoparticles by using glucose as carbon source [141]. The conductive carbon matrix can effectively accelerate the transfer of electron and mitigate the aggregation of $(NH_4)_2V_3O_8$ nanoparticles, thus the proposed $(NH_4)_2V_3O_8$/C cathode exhibits enhanced Zn^{2+} diffusion coefficient ($\sim 10^{-10}$ cm^2/s) and cycling stability (a high reversible capacity of 135 mAh/g could be remained after 2000 cycles at 1 A/g). Though the advantages of numerous carbonaceous materials in promoting electrochemical behaviors of NVO have been verified, the researches pertaining to the positive influence of their structures are still insufficient, and those carbonaceous substrates/architectures with specific structures, such as hollow sphere and core-shell structure, are expected to perform the better Zn^{2+} storage capabilities together.

7. Conclusions and perspectives

The past few years have witnessed the escalating developments in elucidating the potentials of NVO-based cathodes in ZIBs owing to their unique physical and chemical properties. Herein, the state-of-the-art modification strategies of NVO-based materials at the molecular level are systematically summarized, and the relevant electrochemical performances are also compared. As aforementioned, the commonly adopted molecular engineering strategies for NVO can be briefly classified into five categories in general: intercalation engineering, defect engineering, interfacial engineering, doping engineering and structural engineering. The positive influences of each modification strategy are summarized in detail to reveal their unique contributions on NVO, such as tuning the electronic structure, mitigating electrostatic repulsion and inhibiting vanadium dissolution. Note that the Zn^{2+} storage capabilities of NVO-based cathodes can be further optimized by synergistically exploiting multiple molecular engineering strategies. Meanwhile, the deficiencies of these molecular engineering strategies are discussed to clarify the unsolved issues and future research directions. We believe that this review can deepen the researchers' comprehension of the potentials of NVO-based materials, and further facilitating the exploitation of NVO-based cathodes with superb Zn^{2+} storage capabilities and transfer kinetics. Moreover, the summarized molecular engineering strategies of NVO may also suitable for other analogues with typical $[VO]_n$ layered structures, thus further squeezing the merits of vanadium-based cathodes in ZIBs.

As one of the most prevalent models of aqueous batteries, aqueous Zn-MnO_2 battery has made great progress in its commercialization process by virtue of its low cost (less than 70 ¥/kWh), nontoxicity and favorable energy density [142]. However, MnO_2 possesses the comparatively low capacity (~200–300 mAh/g at 0.1 A/g) and inferior cycle lifespan due to the inevitable Mn dissolution. In contrast, NVO-based cathodes generally exhibit the favorable capacities (larger than 400 mAh/g at 0.1 A/g) and power densities, whereas the comparatively high cost of vanadium makes its cost (~300–450 ¥/kWh) far larger than that of MnO_2 [143]. Therefore, to improve the competitiveness of NVO-based cathodes, they need to further reflect their values of high stabilities and power densities, and the relevant modification strategies are required to maintain/promote the above advantages, thus guaranteeing their great potentials in long-duration and high-power-density energy

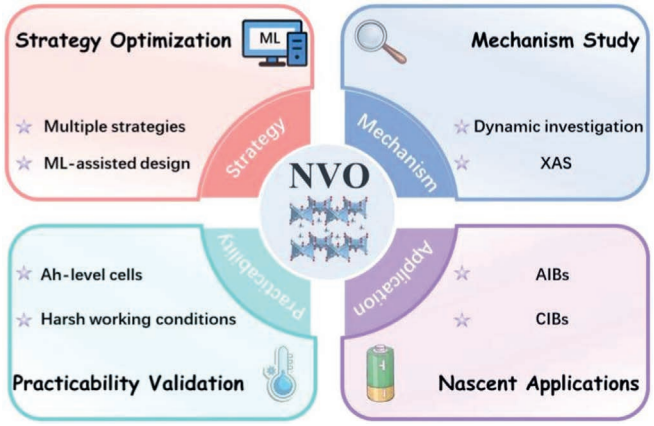


Fig. 12. The promising prospects of NVO-based electrodes in future developments.

storage devices to realize their commercialization values. Notwithstanding the considerable efforts, NVO-based cathodes have not yet reached their full potentials, and some challenges and opportunities need to be further revealed. Based on the previous researches, we herein propose the relevant suggestions as listed below (Fig. 12), and hope they can accelerate the development of NVO-based electrodes in ZIBs and other energy-related fields.

7.1. Strategy optimization

For NVO-based cathodes, the general modification aspects lie in the following points: (1) The overall conductivity; (2) the transfer kinetics of Zn^{2+} in the interfaces and electrolyte; (3) the transfer kinetics of Zn^{2+} in the interlayer of NVO; (4) the structural stability (suppression of vanadium dissolution); (5) the extra active sites for Zn^{2+} storage. Generally, the single molecular engineering strategy can simultaneously realize two or three above goals. For instance, intercalation engineering can simultaneously accelerate the Zn^{2+} transfer kinetics in the interlayer of NVO by expanding its interlayer distance, and strengthen its structural stability by supplying extra interlayer "pillars". The interfacial engineering can not only accelerate the Zn^{2+} transfer kinetics in the interfaces by generating internal electric field or providing more channels for Zn^{2+} to transfer, but also improve the overall conductivity. Though the adoption of single molecular engineering strategy can effectively enhance the Zn^{2+} storage capability of NVO, the proposed electrochemical behaviors are still far from its extremums. Therefore, multiple molecular engineering strategies are desired to simultaneously improve all the five goals of NVO, thus fully digging the potentials of NVO-based cathodes. By utilizing the synergistic effects of those molecular engineering strategies, NVO-based cathodes are expected to possess the significantly boosted electrochemical properties. For instance, Liu *et al.* simultaneously adopted the defect engineering and structural engineering to suppress the vanadium dissolution of $(NH_4)_2V_{10}O_{25}$ and improve its structural stability [91], while Liu *et al.* used the intercalation engineering and defect engineering synchronously to accelerate the Zn^{2+} transfer kinetics of $NH_4V_4O_{10}$ cathode [86], and all the proposed cathodes exhibit the better performances than that of NVO cathodes with single modification strategy, indicating the positive influence of the use of multiple molecular engineering strategies. In addition, several extra advanced modification strategies beyond aforementioned strategies are also proposed recently, such as the electrochemical activation strategy [144], electrode recipe optimization strategy [145], and the *in-situ* phase transformation strategy [146]. Those strategies can promote the Zn^{2+} storage capabilities of NVO from different aspects, and they may be able to collaborate with above molecular engineering strategies to further alleviate the intrinsic drawbacks of vanadium-based cathodes and modulate their electrochemical properties.

In addition, with the rise of advanced computer science, the crucial parameters of molecular engineering strategies of NVO can be further optimized by means of computer science techniques. Usually, the DFT calculations based on the first-principle are often adopted to reveal the mechanism of the enhanced electrochemical properties of NVO, while there is still a lack of the established prediction technology to guide the structure design of NVO-based cathodes. With the rise of computer science, machine learning (ML) technology has been gradually used in the energy-related fields, such as Li-S battery and LIBs [147,148], and guide to the structure optimization of active materials. Specifically, ML technology may be able to be adopted to predict the optimal parameters of aforementioned modification strategies, such as the optimal O/NH_4^+ defect content (defect engineering), the optimal intercalators/intercalation contents (intercalation engineering) and the optimal dopants/doping content (doping engineering) of NVO. However, none of the reported researches pertaining to the NVO-based cathodes used the ML method, and the electrochemical behaviors of NVO-based cathodes guided by the ML technology are highly expected.

7.2. Mechanism study

Advanced characterization technologies are crucial to reveal the structural variation and the structure-function relationships of NVO-based cathodes. However, there is still a lack of papers pertaining to the advanced characterization techniques and dynamic investigation of NVO. In addition to the ordinary characterization technologies (such as XRD, Raman and EPR), more elaborate characterizations, such as X-ray absorption spectroscopy (XAS) [149] and scanning electrochemical microscopy (SECM), are highly desired to further reveal the modified properties of NVO samples. For instance, the X-ray absorption near-edge structure (XANES) spectroscopy can effectively disclose the variation of electronic structure of NVO, thus verifying the positive influences contributed by the defect engineering/intercalation engineering strategies, while the extended X-ray absorption fine structure (EXAFS) spectroscopy can substantiate the change of coordination environment of V atoms to verify the effectiveness of doping engineering strategy. Moreover, the built-in electric field generated by the interfacial engineering strategy can be also witnessed by the SECM technique. Unfortunately, the above advanced characterization techniques are still rarely applied in previous researches pertaining to the modification of NVO-based cathodes.

In addition to the advanced characterization techniques, the dynamic investigations of NVO during the cycling process are also highly required because they can effectively promote the understandings of storage mechanisms and structural evolutions [150]. Though researchers have adopted various *in-situ/ex-situ* technologies (such as XRD, XPS TEM) to monitor the charging/discharging processes of NVO-based cathodes in ZIBs, the merits contributed by those molecular engineering strategies need to be further witnessed during the electrochemical reaction processes. In recent years, *in-situ* X-ray microtomography technology has been widely adopted in LIBs to monitor its lithiation process [151,152]. Similarly, it may be also applied to monitor the intercalation/deintercalation processes of Zn^{2+} in NVO-based cathodes. Moreover, the synchrotron radiation X-ray 3D nano-computed tomography (3D nano-CT) technique is also hired in Li-S battery system to obtain the inner structural variation very recently [153]. The above technologies enable researchers to monitor the electrochemical processes and observe the structural evolution real-timely. Besides, they can also combine with other *in-situ* technologies to

further reveal the metal-ion intercalation/deintercalation processes [154]. The utilization of above advanced dynamic characterizations in ZIBs is expected to greatly strengthen the comprehension of energy storage mechanisms and the merits of molecular engineering strategies of NVO-based cathodes, while there are no relevant reports yet.

7.3. Practicability validation

Industrial practicability is one of the most important characteristics to evaluate the potentials of cathodes in ZIBs [155]. Though the Zn^{2+} storage capabilities of NVO-based cathodes have been extensively studied, their relevant electrochemical properties are generally obtained from the tests of coin cells in most of the reported papers, and their commercial potentials have not been fully revealed. Hence, the electrochemical Zn^{2+} storage capabilities of NVO-based cathodes that based on the tests of Ah-level pouch batteries are highly expected, while only a few papers have indicated the application potentials of NVO in pouch batteries yet [156].

The working reliability under the wide-temperature-range conditions is another crucial parameter to assess the commercial practicability of electrode. Specifically, the low working temperature can significantly decelerate the transfer kinetics of Zn^{2+} (especially at the CEI) in ZIBs, thus resulting in the inferior transfer kinetics and electrochemical properties [157]. Due to the university of the working conditions at low temperature (such as high-latitude area, abysmal region and outer space), squeezing the application potentials of NVO-based cathodes at low-temperature conditions is crucial to accelerate the commercialization progress of NVO. He *et al.* adopted the defect engineering strategy to fabricate the $NH_4V_4O_{10-x}{\cdot}nH_2O$ microspheres serving as cathode for ZIBs [85]. With an oxygen-deficient ratio of ~1.5%, the proposed $NH_4V_4O_{10-x}{\cdot}nH_2O$ possesses a high capacity of 329.3 mAh/g after 100 cycles at 0.1 A/g under the condition of −30 °C (about 95.8% of its capacity at room temperature), indicating its favorable tolerance to low-temperature condition. Ren *et al.* used structural engineering strategy to constructed the 3D hierarchical $NH_4V_4O_{10}$ microsphere, and it maintains ~90 mAh/g after 3000 cycles at 5 A/g [135]. However, in consideration of the retarded Zn^{2+} transfer kinetics at the CEI, the interfacial engineering strategy may be one of the most effective ways to alleviate the drawbacks caused by the severe conditions, while it has not been verified yet. By rationally constructing the multi-field coupling (such as magnetic field and piezoelectricity field)/conductive interfaces, NVO-based cathodes are expected to perform the better Zn^{2+} transfer kinetics and electrochemical properties at low-temperature condition. In addition, it is suggested that the optimization of solvation sheath structure in electrolyte can also accelerate the Zn^{2+} transfer kinetics and promote the low-temperature Zn^{2+} storage capability of $NH_4V_4O_{10}$ [158]. Therefore, by combining the molecular engineering strategies of NVO cathode and the electrolyte engineering strategies, the promising electrochemical properties of NVO-based cathodes at low-temperature condition are highly expected. Besides, the electrochemical performance of NVO under high-temperature condition is also important for its commercialization. However, only one paper reported its performance under high-temperature condition (a capacity of ~400 mAh/g can be retained after 100 cycles at 5 A/g and 50 °C for $NH_4V_4O_{10}$ cathode) [135], and more researches are needed to further reveal and optimize their electrochemical properties at harsh working conditions to further promote its commercialization value.

7.4. Emerging applications

As aforementioned, NVO-based electrodes have been extensively adopted in various metal-ion batteries, such as LIBs and PIBs [130], by virtue of their comparatively larger interlayer distances and stability layered structures. Recently, ammonium-ion batteries (AIBs) have gained tremendous attentions because of the inherent safety and smaller hydration radius (3.31 Å) of the NH_4^+ charge carriers [159]. In view of the successful applications of NVO-based electrodes in ZIBs and other metal-ion batteries, the using of NVO-based hosts in AIBs is on the agenda. Compared to other host materials, NVO owns larger interlayer distance and its $[VO]_n$ layers can provide numerous sites to store the ammonium-ions *via* hydrogen bonds, thus exhibiting the great potentials in AIBs. Very recently, Krishnan *et al.* proposed a $NH_4V_4O_{10}$/MXene nanocomposite serving as NH_4^+ host material, and it can maintain a high capacity retention of ~98% after 5000 cycles at 1 mA/cm^2 [160]. However, the relevant papers are still insufficient, and the storage mechanisms of NVO-based electrodes need to be further elucidated. Based on their application cases in ZIBs, it can be concluded that those proposed molecular engineering strategies may also applicable for the NVO electrodes in AIBs. For instance, adopting the defect engineering to partially remove its interlayer ammonium-ions can provide more space to store the external ammonium-ions, introducing appropriate heteroatoms (such as N) *via* doping engineering can endow NVO with more active sites to form hydrogen bonds with NH_4^+ and thereby increasing the ammonium-ion storage capacity, and the using of structural engineering strategy can improve the active surface area of NVO and significantly improve the pseudocapacitive storage capacity of NH_4^+. Hence, the great potentials of NVO in AIBs are expected by rationally adopting the molecular engineering strategies. Moreover, the merits of NVO-based electrodes in the emerging calcium-ion batteries (CIBs) are preliminarily revealed recently [161]. Wang *et al.* proposed a free-standing $(NH_4)_2V_6O_{16}$@GO@CNT composite serving as the cathode of CIBs, and it can deliver a favorable capacity of 134.9 mAh/g after 300 cycles at 0.1 A/g [162]. However, the positive influences contributed by molecular engineering strategies and the storage mechanisms of NVO-based cathodes still remain to be revealed due to the lack of related papers, and we believe this review would further accelerate the exploration of NVO-based electrodes in CIBs and other emerged energy-related applications.

Declaration of competing interest

The authors declare that they have no known competing financial interests or personal relationships that could have appeared to influence the work reported in this paper.

CRediT authorship contribution statement

Kang Zhang: Writing – original draft, Data curation, Conceptualization. **Jin Zhao:** Writing – original draft, Formal analysis, Data curation, Conceptualization. **Pengcheng Su:** Formal analysis, Data curation. **Mingkun Wang:** Formal analysis, Data curation. **Kexin Wan:** Conceptualization. **Hongwei Tang:** Writing – review & editing. **Dai-Huo Liu:** Writing – review & editing, Formal analysis. **Jingyu Sun:** Writing – review & editing, Funding acquisition, Formal analysis. **Yihui Li:** Writing – review & editing, Funding acquisition, Conceptualization.

References

[1] D. Griggs, M. Stafford-Smith, O. Gaffney, et al., Nature 495 (2013) 305.
[2] Y. Liang, H. Dong, D. Aurbach, Y. Yao, Nat. Energy 5 (2020) 646–656.
[3] Z. Zeng, B. Ran, M. Cui, F. Liu, Y. Huang, ChemNanoMat 11 (2025) e202400631.
[4] M. Li, J. Lu, Z. Chen, K. Amine, Adv. Mater. 30 (2018) 1800561.
[5] C. Li, S. Jin, L.A. Archer, L.F. Nazar, Joule 6 (2022) 1733–1738.
[6] Z. Yi, G. Chen, F. Hou, L. Wang, J. Liang, Adv. Energy Mater. 11 (2021) 2003065.
[7] G. Fang, J. Zhou, A. Pan, S. Liang, ACS Energy Lett. 3 (2018) 2480–2501.
[8] N. Zhang, F. Cheng, J. Liu, et al., Nat. Commun. 8 (2017) 405.
[9] Y. Li, Z. Lu, J. Liu, Y. Huang, Device 3 (2025) 100641.

[10] N. Zhang, Y. Dong, M. Jia, et al., ACS Energy Lett. 3 (2018) 1366–1372.
[11] H. Tang, K. Wan, K. Zhang, et al., ACS Sustainable Chem. Eng. 12 (2024) 13848–13860.
[12] H. Liu, X. Hou, T. Fang, et al., Energy Storage Mater. 55 (2023) 279–288.
[13] S. Zhou, X. Wu, H. Du, et al., J. Colloid Interface Sci. 623 (2022) 456–466.
[14] H. Huang, H. Feng, Z. He, et al., ACS Nano 18 (2024) 25601–25613.
[15] X. Zhu, Z. Cao, W. Wang, et al., ACS Nano 15 (2021) 2971–2983.
[16] T.W. Lin, M.S. Kumar, H.H. Shen, J.Y. Lin, J. Power Sources 614 (2024) 234972.
[17] M. Zhang, W. Zhao, T. Yang, et al., Adv. Energy Mater. 14 (2024) 2400543.
[18] H. Liang, Z. Cao, F. Ming, et al., Nano Lett. 19 (2019) 3199–3206.
[19] Y. Li, X. Dong, Z. Xu, et al., Adv. Mater. 35 (2023) 2208615.
[20] S. Li, Y. Liu, X. Zhao, et al., Angew. Chem. Int. Ed. 60 (2021) 20286–20293.
[21] W. Wang, V.S. Kale, Z. Cao, et al., Adv. Mater. 33 (2021) 2103617.
[22] S. Haldar, A. Schneemann, S. Kaskel, J. Am. Chem. Soc. 145 (2023) 13494–13513.
[23] F. Ye, Q. Liu, H. Dong, et al., Angew. Chem. Int. Ed. 61 (2022) e202214244.
[24] P. Hu, M. Yan, T. Zhu, et al., ACS Appl. Mater. Inter. 9 (2017) 42717–42722.
[25] Y. Ding, Y. Peng, S. Chen, et al., ACS Appl. Mater. Inter. 11 (2019) 44109–44117.
[26] J. Shin, D.S. Choi, H.J. Lee, Y. Jung, J.W. Choi, Adv. Energy Mater. 9 (2019) 1900083.
[27] X. Wang, B. Xi, X. Ma, et al., Nano Lett. 20 (2020) 2899–2906.
[28] G. Wang, B. Guan, J. Wang, et al., ACS Appl. Mater. Inter. 16 (2024) 66018–66031.
[29] S. Li, X. Xu, K. Wang, et al., ACS Energy Lett. 7 (2022) 3770–3779.
[30] B. Tang, J. Zhou, G. Fang, et al., J. Mater. Chem. A 7 (2019) 940–945.
[31] X. Wang, B. Xi, Z. Feng, et al., J. Mater. Chem. A 7 (2019) 19130–19139.
[32] H.Y. Shi, Y. Song, Z. Qin, et al., Angew. Chem. Int. Ed. 58 (2019) 16057–16061.
[33] G. Li, Z. Yang, Y. Jiang, et al., Nano Energy 25 (2016) 211–217.
[34] P. Hu, T. Zhu, X. Wang, et al., Nano Energy 58 (2019) 492–498.
[35] W. Zheng, X. Hu, M. Wu, et al., Chem. Eng. J. 454 (2023) 140194.
[36] H. Chen, Z. Sun, C. Wang, et al., J. Mater. Chem. C 5 (2017) 4185–4189.
[37] H. Jiang, Y. Zhang, Z. Pan, et al., Electrochim. Acta 332 (2020) 135506.
[38] Y. Cheng, J. Huang, J. Li, et al., Electrochim. Acta 212 (2016) 217–224.
[39] A. Sarkar, S. Sarkar, T. Sarkar, et al., ACS Appl. Mater. Inter. 7 (2015) 17044–17053.
[40] C. Chen, Q. Deng, Q. Zhang, et al., J. Colloid Interface Sci. 633 (2023) 619–627.
[41] Q. Zhou, Y. Gong, J. Lin, Appl. Surf. Sci. 439 (2018) 33–44.
[42] J. Lai, H. Tang, X. Zhu, Y. Wang, J. Mater. Chem. A 7 (2019) 23140–23148.
[43] Z. Wang, J. Zhang, H. Wang, et al., Electrochim. Acta 404 (2022) 139785.
[44] R. Wei, X. Wang, B. Xi, et al., ACS Appl. Energy Mater. 3 (2020) 5343–5352.
[45] K. Fang, H. Zhang, P. Chen, et al., Chem. Eng. J. 496 (2024) 153736.
[46] Y. Liu, X. Wu, J. Energy Chem. 56 (2021) 223–237.
[47] Y. Li, M. Wang, J. Sun, Adv. Energy Mater. 12 (2022) 2202600.
[48] Q. Zhao, A. Song, S. Ding, et al., Adv. Mater. 32 (2020) 2002450.
[49] Y. Fan, Z. Qu, W. Zhong, ACS Appl. Mater. Inter. 13 (2021) 7377–7388.
[50] J. Cao, T. Ou, Y. Sun, et al., J. Colloid Interface Sci. 665 (2024) 32–40.
[51] L. Zhang, R. Wang, M. Wang, D. Fang, J. Yi, Chem. Eng. J. 475 (2023) 146127.
[52] J. Chen, Y. Zhai, Y. Li, et al., Small 20 (2024) 2309412.
[53] X. Wang, A. Naveed, T. Zeng, et al., Chem. Eng. J. 446 (2022) 137090.
[54] Z. Wang, H. Wang, X. Bai, et al., ACS Appl. Nano Mater. 7 (2024) 27090–27099.
[55] K. Wang, S. Li, X. Chen, et al., ACS Nano 18 (2024) 7311–7323.
[56] Q. Zong, Q. Wang, C. Liu, et al., ACS Nano 16 (2022) 4588–4598.
[57] Z. Deng, W. Shao, H. Wang, et al., J. Power Sources 614 (2024) 234976.
[58] H. Tang, F. Chao, H. Luo, et al., ChemSusChem 16 (2023) e202300403.
[59] H. Yao, L. Yang, Z. Li, et al., ACS Sustain. Chem. Eng. 12 (2024) 13274–13284.
[60] Z. Fang, Y. Tong, Y. Yang, et al., Inorg. Chem. Front. 11 (2024) 8855–8865.
[61] Z. Dai, C. Yang, J. Cao, et al., Chem. Eng. J. 516 (2025) 164027.
[62] P. Tian, Y. Gao, S. Huang, et al., Adv. Energy Mater. 14 (2024) 2401830.
[63] C. Zhang, Y. Huang, X. Xu, et al., Energy Environ. Sci. 17 (2024) 4090–4103.
[64] L. Zhang, B. Zhang, J. Hu, et al., Small Methods 5 (2021) 2100094.
[65] Z. Yao, W. Zhang, X. Ren, et al., ACS Nano 16 (2022) 12095–12106.
[66] Q. Zong, Y. Zhuang, C. Liu, et al., Adv. Energy Mater. 13 (2023) 2301480.
[67] J. Chen, L. Su, X. Zhang, et al., ACS Sustainable Chem. Eng. 11 (2023) 12467–12476.
[68] C. Lu, Z. Yang, Y. Wang, et al., Chin. Chem. Lett. 34 (2023) 108572.
[69] H. Tang, K. Wan, K. Zhang, et al., ACS Nano 18 (2024) 30896–30909.
[70] S. Kong, Y. Li, X. Zhang, et al., Small 19 (2023) 2304462.
[71] J. Chen, X. Zhang, Y. Li, et al., J. Mater. Chem. A 12 (2024) 28119–28129.
[72] S.H. Lee, C. Park, J.W. Park, et al., J. Power Sources 414 (2019) 460–469.
[73] S. Zhao, S. Wang, J. Guo, et al., Adv. Funct. Mater. 33 (2023) 2305700.
[74] Y. Li, Y. Liu, J. Chen, et al., Chem. Eng. J. 448 (2022) 137681.
[75] W. Kang, B. Zhang, Z. Wang, et al., J. Energy Chem. 94 (2024) 608–617.
[76] L. Chen, Z. Zhang, Y. Ma, et al., Inorg. Chem. Front. 10 (2023) 1926–1937.
[77] Y. Gong, P. Zhang, S. Fan, et al., J. Colloid Interface Sci. 664 (2024) 168–177.
[78] X. Cai, Y. Zhang, H. Cheng, et al., Small 19 (2023) 2304668.
[79] D. Bin, W. Huo, Y. Yuan, et al., Chem 6 (2020) 968–984.
[80] J. Kim, S.H. Lee, C. Park, et al., Adv. Funct. Mater. 31 (2021) 2100005.
[81] M. Li, M. Liu, Y. Lu, et al., Adv. Funct. Mater. 34 (2024) 2312789.
[82] Y. Xu, G. Fan, P.X. Sun, et al., Angew. Chem. Int. Ed. 62 (2023) e202303529.
[83] Y. Qiu, Z. Sun, Z. Guo, et al., Small 20 (2024) 2311029.
[84] Y. Liu, Z. Feng, H. Jiang, et al., Green Energy Environ. 9 (2024) 1171–1182.
[85] T. He, Y. Ye, H. Li, et al., Mater. Today 43 (2021) 53–61.
[86] C. Liu, Y. Zhang, H. Cheng, et al., Small 19 (2023) 2301870.
[87] S. Yao, Y. Sun, L. Pan, Appl. Surf. Sci. 672 (2024) 160785.
[88] L. Chen, H. Yue, Z. Zhang, et al., Chem. Eng. J. 455 (2023) 140679.
[89] Q. Zong, W. Du, C. Liu, et al., Nano-Micro Lett. 13 (2021) 116.
[90] Y. Zheng, C. Tian, Y. Wu, et al., Energy Storage Mater. 52 (2022) 664–674.
[91] G.L. Liu, T. Zhang, X.J. Li, et al., Rare Met. 42 (2023) 3729–3740.
[92] J. Qi, Y. Zhang, M. Li, et al., J. Colloid Interface Sci. 642 (2023) 430–438.
[93] J. Cao, D. Zhang, Y. Yue, et al., Nano Energy 84 (2021) 105876.
[94] Y. Bai, H. Zhang, Q. Hu, Y. Zhou, B. Xiang, Nano Energy 90 (2021) 106596.
[95] Y. Zou, W. Zhang, N. Chen, et al., ACS Nano 13 (2019) 2062–2071.
[96] M. Liao, J. Wang, L. Ye, et al., Angew. Chem. Int. Ed. 59 (2020) 2273–2278.
[97] S. Li, X. Xu, W. Chen, et al., Energy Storage Mater. 65 (2024) 103108.
[98] B. Chen, S. Sui, F. He, et al., Chem. Soc. Rev. 52 (2023) 7802–7847.
[99] X.L. Xie, S. Wang, D.W. Gu, et al., ACS Appl. Mater. Inter. 16 (2024) 8679–8687.
[100] X. Song, X. Li, H. Shan, et al., Adv. Funct. Mater. 34 (2024) 2303211.
[101] J. Lai, A. Nsabimana, R. Luque, G. Xu, Joule 2 (2018) 76–93.
[102] X. Li, L. Zhi, Chem. Soc. Rev. 47 (2018) 3189–3216.
[103] Z. Pan, Q. Ru, M. Zheng, et al., ChemElectroChem 8 (2021) 4618–4624.
[104] Y. Jiang, Z. Wu, F. Ye, et al., Energy Storage Mater. 42 (2021) 286–294.
[105] H. Jiang, Y. Zhang, Y. Liu, et al., J. Mater. Chem. A 8 (2020) 15130–15139.
[106] L. Liu, K. Chen, Z. Li, W. Huang, ACS Appl. Energy Mater. 6 (2023) 8634–8643.
[107] F. Cui, D. Wang, F. Hu, et al., Energy Storage Mater. 44 (2022) 197–205.
[108] Q. Li, J. Lin, S. Shen, et al., Small 21 (2025) 2500767.
[109] Y. Ran, M. Li, H. Zhao, et al., Adv. Funct. Mater. 35 (2025) e10241.
[110] X. Wang, Y. Wang, Y. Jiang, et al., Adv. Funct. Mater. 31 (2021) 2103210.
[111] W. Nie, J. Sun, S. Xu, et al., Chem. Eng. J. 478 (2023) 147385.
[112] S. Lee, J. Hwang, C. Park, et al., Appl. Surf. Sci. 641 (2023) 158467.
[113] J. Pang, R.G. Mendes, A. Bachmatiuk, et al., Chem. Soc. Rev. 48 (2019) 72–133.
[114] J. Qi, Y. Zhang, J. Wen, et al., J. Colloid Interface Sci. 652 (2023) 285–293.
[115] Y. Fang, C. Qi, W. Bao, et al., Energy Environ. Sci. 18 (2025) 367–377.
[116] Y. Li, M. Chen, B. Liu, et al., Adv. Energy Mater. 10 (2020) 2000927.
[117] Y. Chen, C. Lin, X. Chen, et al., Adv. Energy Mater. 14 (2024) 2304303.
[118] H. Geng, M. Cheng, B. Wang, et al., Adv. Funct. Mater. 30 (2020) 1907684.
[119] S. Kim, B.R. Koo, Y.R. Jo, et al., J. Mater. Chem. A 9 (2021) 17211–17222.
[120] W. Cao, Z. Chen, J. Chen, et al., Mater. Today 77 (2024) 118–141.
[121] X. Wang, Y. Wang, A. Naveed, et al., Adv. Funct. Mater. 33 (2023) 2306205.
[122] D. He, Y. Peng, Y. Ding, et al., J. Power Sources 484 (2021) 229284.
[123] H. Wang, R. Jing, J. Shi, et al., J. Alloys Compd. 858 (2021) 158380.
[124] Y. Zhuang, Q. Zong, Y. Wu, et al., Small 20 (2024) 2306561.
[125] S. Deng, X. Yan, Y. Jiang, et al., Chem. Eng. J. 503 (2025) 158472.
[126] R. Monsef, M. Salavati-Niasari, J. Energy Storage 74 (2023) 109395.
[127] D. Fang, Y. Cao, R. Liu, et al., Appl. Surf. Sci. 360 (2016) 658–665.
[128] A. Ottmann, G.S. Zakharova, B. Ehrstein, R. Klingeler, Electrochim. Acta 174 (2015) 682–687.
[129] H. Wang, K. Huang, Y. Ren, et al., J. Power Sources 196 (2011) 9786–9791.
[130] H. Wang, Y. Ren, W. Wang, et al., J. Power Sources 199 (2012) 315–321.
[131] X. Jia, C. Liu, Z.G. Neale, J. Yang, G. Cao, Chem. Rev. 120 (2020) 7795–7866.
[132] M. Tamilselvan, T.V.M. Sreekanth, K. Yoo, J. Kim, J. Alloys Compd. 876 (2021) 160130.
[133] Y. Lu, Z. Wang, M. Li, et al., Adv. Funct. Mater. 34 (2024) 2310966.
[134] Q. Li, X. Rui, D. Chen, et al., Nano-Micro Lett. 12 (2020) 67.
[135] X. Ren, Z. Gan, M. Liu, et al., J. Power Sources 622 (2024) 235370.
[136] G. Li, Y. Su, S. Zhou, et al., Chem. Eng. J. 469 (2023) 143816.
[137] R. Sun, Z. Qin, X. Liu, et al., ACS Sustain. Chem. Eng. 9 (2021) 11769–11777.
[138] X. Du, H. Wang, X. Cui, et al., Appl. Surf. Sci. 610 (2023) 155408.
[139] J. Lu, X. Zhong, X. Lin, et al., Energy Environ. Sci. 17 (2024) 6833–6843.
[140] F. Hu, Y. Gu, F. Cui, G. Song, K. Zhu, Chin. Chem. Lett. 32 (2021) 3793–3798.
[141] H. Jiang, Y. Zhang, L. Xu, et al., Chem. Eng. J. 382 (2020) 122844.
[142] T. Xue, H.J. Fan, J. Energy Chem. 54 (2021) 194–201.
[143] X. Wang, Z. Zhang, B. Xi, et al., ACS Nano 15 (2021) 9244–9272.
[144] K. Fang, Y.L. Liu, P. Chen, et al., Nano Energy 114 (2023) 108671.
[145] C. Huang, S. Liu, J. Feng, et al., J. Power Sources 490 (2021) 229528.
[146] L. Chen, Y. Zheng, Z. Zhang, et al., Inorg. Chem. Front. 11 (2024) 1266–1278.
[147] H. Zhang, Z. Wang, J. Ren, J. Liu, J. Li, Energy Storage Mater. 35 (2021) 88–98.
[148] J. Sturman, C.H. Yim, E.A. Baranova, Y. Abu-Lebdeh, J. Electrochem. Soc. 168 (2021) 050541.
[149] M. Nadolska, M. Szkoda, K. Trzciński, et al., Sci. Rep. 13 (2023) 3946.
[150] C. Zeng, J. Liang, C. Cui, T. Zhai, H. Li, Adv. Mater. 34 (2022) 2200777.
[151] A.S. Ho, D.Y. Parkinson, D.P. Finegan, et al., ACS Nano 15 (2021) 10480–10487.
[152] A. Mistry, K. Smith, P.P. Mukherjee, ACS Appl. Mater. Inter. 12 (2020) 16359–16366.
[153] Q. Yang, C. Wang, L. Song, Y. Zhang, Z. Shen, et al., Angew. Chem. Int. Ed. 64 (2025) e202415078.
[154] L. Hong, L. Li, Y.K. Chen-Wiegart, et al., Nat. Commun. 8 (2017) 1194.
[155] Y. Ren, H. Li, Y. Rao, H. Zhou, S. Guo, Energy Environ. Sci. 17 (2024) 425–441.
[156] S. Li, Y. Zhong, J. Huang, et al., Energy Environ. Sci. 18 (2025) 8256.
[157] L. Jia, H. Hu, X. Cheng, et al., Adv. Energy Mater. 14 (2024) 2304010.
[158] Y. He, Z. Chen, J. Feng, et al., Small 21 (2025) 2411755.
[159] R. Zhang, S. Wang, S. Chou, H. Jin, Adv. Funct. Mater. 32 (2022) 2112179.
[160] S.G. Krishnan, C. Padwal, X. Wang, et al., J. Mater. Chem. A 12 (2024) 8244–8253.
[161] H. Bu, H. Lee, J. Hyoung, et al., Chem. Mater. 35 (2023) 7974–7983.
[162] J. Wang, Y. Zhang, F. Qiao, et al., Adv. Mater. 36 (2024) 2403371.